CORONAVIRUS

ZBP1-dependent inflammatory cell death, PANoptosis, and cytokine storm disrupt IFN therapeutic efficacy during coronavirus infection

Rajendra Karki[1]†, SangJoon Lee[1]†‡, Raghvendra Mall[1], Nagakannan Pandian[1], Yaqiu Wang[1], Bhesh Raj Sharma[1], RK Subbarao Malireddi[1], Dong Yang[2], Sanja Trifkovic[3], Jacob A. Steele[4], Jon P. Connelly[4], Gella Vishwanath[5], Mitnala Sasikala[6], Duvvur Nageshwar Reddy[7], Peter Vogel[8], Shondra M. Pruett-Miller[4], Richard Webby[3], Colleen Beth Jonsson[9], Thirumala-Devi Kanneganti[1]*

Severe acute respiratory syndrome coronavirus 2 (SARS-CoV-2), the virus responsible for coronavirus disease 2019 (COVID-19), continues to cause substantial morbidity and mortality in the ongoing global pandemic. Understanding the fundamental mechanisms that govern innate immune and inflammatory responses during SARS-CoV-2 infection is critical for developing effective therapeutic strategies. Whereas interferon (IFN)–based therapies are generally expected to be beneficial during viral infection, clinical trials in COVID-19 have shown limited efficacy and potential detrimental effects of IFN treatment during SARS-CoV-2 infection. However, the underlying mechanisms responsible for this failure remain unknown. In this study, we found that IFN induced Z-DNA-binding protein 1 (ZBP1)–mediated inflammatory cell death, PANoptosis, in human and murine macrophages and in the lungs of mice infected with β-coronaviruses, including SARS-CoV-2 and mouse hepatitis virus (MHV). In patients with COVID-19, expression of the innate immune sensor *ZBP1* was increased in immune cells from those who succumbed to the disease compared with those who recovered, further suggesting a link between ZBP1 and pathology. In mice, IFN-β treatment after β-coronavirus infection increased lethality, and genetic deletion of *Zbp1* or its Zα domain suppressed cell death and protected the mice from IFN-mediated lethality during β-coronavirus infection. Overall, our results identify that ZBP1 induced during coronavirus infection limits the efficacy of IFN therapy by driving inflammatory cell death and lethality. Therefore, inhibiting ZBP1 activity may improve the efficacy of IFN therapy, paving the way for the development of new and critically needed therapeutics for COVID-19 as well as other infections and inflammatory conditions where IFN-mediated cell death and pathology occur.

INTRODUCTION

Coronavirus disease 2019 (COVID-19), caused by severe acute respiratory syndrome coronavirus 2 (SARS-CoV-2) infection, has led to substantial mortality, morbidity, and global socioeconomic and psychological distress (*1*, *2*). Severe cases of COVID-19 are characterized by acute respiratory distress syndrome, multiorgan failure, and death (*3*, *4*). Innate immunity is the first line of host defense against invading viruses, including SARS-CoV-2. Conserved cellular receptors in innate immune cells detect viral DNA and RNA and rapidly induce interferon (IFN) production, which subsequently up-regulates numerous IFN-stimulated genes (ISGs) to limit viral replication

(*5*, *6*). However, SARS-CoV-2 can evade antiviral responses by actively interfering with IFN production (*7–17*), and the sera of patients with mild or moderate COVID-19 has similar levels of type I and III IFNs compared with those of healthy patients (*18*). To counteract these evasion mechanisms, IFN treatment has been considered as a therapeutic option for patients with COVID-19. In preclinical studies, treatment with exogenous type I IFNs or agonists that induce type I IFN reduces viral load when administered before SARS-CoV-2 infection (*19–22*), but this effect is limited once infection is established (*23*). These observations suggest that IFN-based therapies have prophylactic, but limited therapeutic, potential. Moreover, the use of IFN-based therapy in the treatment of patients with COVID-19 has yielded mixed results (*24*, *25*). The World Health Organization (WHO) Solidarity Trial Consortium clinical trial found that type I IFN treatment is not beneficial in treating SARS-CoV-2 infection (*24*). In addition, a retrospective study found that administration of IFN-α2b within 5 days of hospitalization is associated with a decrease in mortality, whereas later administration is associated with increased mortality (*25*). Patients with severe COVID-19 are also reported to have increased IFN levels in their sera compared with those with mild infection (*26*). Together, these findings indicate that IFN-based therapy may only be beneficial to a certain subset of patients when administered early during the infection and needs to be balanced to avoid pathogenic effects. However, determining the optimal time frame for safe and effective IFN therapy is challenging. Therefore, gaining further insights into the molecular mechanisms of IFN signaling during SARS-CoV-2 infection is essential to

[1]Department of Immunology, St. Jude Children's Research Hospital, Memphis, TN 38105, USA. [2]UTHSC Regional Biocontainment Laboratory, University of Tennessee Health Science Center, Memphis, TN 38163, USA. [3]Department of Infectious Diseases, St. Jude Children's Research Hospital, Memphis, TN 38105, USA. [4]Center for Advanced Genome Engineering (CAGE), St. Jude Children's Research Hospital, Memphis, TN 38105, USA. [5]Institute of Pulmonary Medicine and Sleep Disorders, Continental Hospitals, Asian Institute of Gastroenterology, Hyderabad, India. [6]Department of Basic Science, Asian Healthcare Foundation, Asian Institute of Gastroenterology, Hyderabad, India. [7]Department of Medical Gastroenterology, Asian Institute of Gastroenterology, Hyderabad, India. [8]Animal Resources Center and the Veterinary Pathology Core, St. Jude Children's Research Hospital, Memphis, TN 38105, USA. [9]Department of Microbiology, Immunology, and Biochemistry, University of Tennessee Health Science Center, Memphis, TN 38163, USA.
*Corresponding author. Email: thirumala-devi.kanneganti@stjude.org
†These authors contributed equally to this work.
‡Present address: Department of Biological Sciences, Ulsan National Institute of Science and Technology (UNIST), Ulsan, Republic of Korea.

inform clinical protocols and improve the efficacy of IFN therapy in COVID-19.

IFN signaling has multiple roles in response to viral infection. In addition to inducing ISGs that have antiviral properties (27), IFN signaling also up-regulates ISGs that trigger cell death (28, 29). In COVID-19, there is a positive feedback loop between excessive cell death and IFN signaling that leads to cytokine storm, contributing to multiorgan damage as well as clinical features of disease and mortality (4, 30). Therefore, it is important to understand the connection between IFN, cell death, and pathology during SARS-CoV-2 infection to identify ways to maximize the efficacy of IFN-based therapeutic strategies.

One critical ISG that plays a role in cell death during other viral infections is Z-DNA–binding protein 1 (ZBP1), and its complex roles in innate immunity and inflammatory cell death have recently been found. During viral infection or IFN-β treatment, ZBP1 is up-regulated in an IFNAR-dependent manner (29, 31). Sensing of viral and endogenous Z-nucleic acids by the ZBP1 Zα domain allows ZBP1 to interact with RIPK3 via RHIM-RHIM homotypic interactions, thereby activating inflammatory cell death, PANoptosis (29, 31–34). In contrast, up-regulation of ZBP1 by IFN-β treatment alone is not sufficient to induce cell death (29). Whether ZBP1 has a role in driving the pathology during severe COVID-19 or whether it has an impact on the efficacy of IFN-based therapies is not known. Here, using CRISPR-CAS9 knockout (KO) screening and the analysis of multiple publicly available RNA sequencing (RNA-seq) datasets, we identified ZBP1 as a critical cytosolic sensor that drives inflammatory cell death in response to IFN therapy during β-coronavirus infections, including SARS-CoV-2 and mouse hepatitis virus (MHV) infections. IFN-β treatment during SARS-CoV-2 and MHV infections induced robust ZBP1-dependent inflammatory cell death, PANoptosis, in macrophages. In addition, single-cell transcriptomic analysis showed that ZBP1 was more abundantly expressed in immune cells from patients who succumbed to COVID-19 than in those who recovered without needing hospitalization. Furthermore, genetic deletion of Zbp1 or its Zα domain protected mice from the lethality induced by IFN treatment during β-coronavirus infection. These findings suggest that inhibiting ZBP1 activity could improve the efficacy of IFN therapy during β-coronavirus infection. This improved understanding of the fundamental mechanisms engaged by innate immune receptors in inducing inflammatory responses and PANoptosis during SARS-CoV-2 infection is essential to inform the development of effective therapeutic strategies for the treatment of not only COVID-19 but also other infections and inflammatory diseases.

RESULTS

IFN response is delayed during infection with β-coronavirus

Understanding the differentially regulated pathways in patients with varying severities of COVID-19 is critical to identifying the molecular mechanisms that drive pathogenesis of severe SARS-CoV-2 infection. Using a publicly available dataset, we performed pathway analysis to determine the differentially regulated pathways in noncritically ill (NCI) and critically ill (CI) patients with COVID-19 (35). We found that the IFN-α and IFN-γ response pathways were highly enriched in both NCI and CI patients with COVID-19 compared with healthy patients (fig. S1A). Moreover, among the hallmark pathways (36, 37) (see Materials and Methods), IFN-α response was the topmost enriched pathway in CI patients compared with NCI patients with

COVID-19 (Fig. 1A). We also analyzed the IFN responses to determine differentially regulated ISGs during SARS-CoV-2 infection. Several ISGs were up-regulated in CI patients with COVID-19 compared with healthy patients or NCI patients with COVID-19 (fig. S1B). Among the ISGs up-regulated, most of them, including BATF2, PARP9, DDX60, IFIT3, and IFI44, have been reported to have antiviral properties (27, 38, 39), whereas some are involved in inducing cell death, such as EIF2AK2 (28) and ZBP1 (29, 31, 32). However, pathway analysis of whole blood transcriptomes showed that IFN responses in patients with COVID-19 were not as robust as in patients with influenza or sepsis (fig. S2) (40). Because IFNs can have both beneficial and detrimental effects depending on the context (41), we sought to determine the effect of IFNs on cell death during infections with β-coronaviruses and influenza A virus (IAV). Murine bone marrow–derived macrophages (BMDMs) infected with MHV, a prototypical virus of the β-coronavirus genus that mimics many of the key aspects of human β-coronavirus biology, showed delayed dynamics of IFN-β release and signal transducer and activator of transcription 1 (STAT1) activation and reduced ISG up-regulation compared with IAV-infected cells (Fig. 1, B and C). We also found that SARS-CoV-2–infected human THP-1 cells showed delayed IFN responses compared with IAV-infected cells (Fig. 1, B and C). In addition, analysis of public datasets (42, 43) showed early induction of both IFN-α and IFN-γ responses in the lung tissue–derived epithelial cell line Calu-3 upon infection with IAV compared with Calu-3 cells infected with SARS-CoV-2 (Fig. 1D). Moreover, patients with COVID-19 are known to exhibit markedly delayed IFN induction (40). Together, these data suggest that IFN responses are delayed during β-coronavirus infection.

IFN treatment contributes to cell death and lethality during β-coronavirus infection

Because IFN responses are reduced in patients with mild and moderate COVID-19 (18, 40), IFN therapy has been suggested as a treatment strategy for patients with COVID-19. However, IFN-based therapy is beneficial only when administered before the onset of clinical symptoms (25). On the other hand, delayed IFN-β treatment is pathogenic in a mouse model of Middle East respiratory syndrome coronavirus (MERS-CoV) infection (44), and administration of IFN-α2b later than 5 days after hospitalization in patients with SARS-CoV-2 is associated with increased mortality (25), suggesting that the timing of the IFN response relative to virus replication dictates the outcome. To investigate the beneficial or pathological effects of IFN therapy during β-coronavirus infection, we evaluated the effect of IFN treatment during infection in mice. Because infection with β-coronaviruses induced delayed IFN responses (Fig. 1, B to D) and because we wanted to mimic the increased IFN responses observed in CI patients with COVID-19 (Fig. 1A), we treated MHV-infected or SARS-CoV-2–infected wild-type (WT) mice with recombinant IFN-β and examined the pathology and lethality. MHV-infected mice were dosed with IFN-β on days 1 and 3 after infection, and SARS-CoV-2–infected mice were dosed on days 2 and 4 after infection. Whereas 50 to 60% of WT mice infected with the median lethal dose (LD_{50}) of MHV survived (Fig. 2A and fig. S3A), all the MHV-infected WT mice receiving IFN-β succumbed to infection within 7 days (Fig. 2A). Moreover, 63% of the SARS-CoV-2–infected WT mice receiving IFN-β succumbed to infection within 5 days (Fig. 2B), suggesting that IFN-β treatment contributes to lethality during β-coronavirus infection.
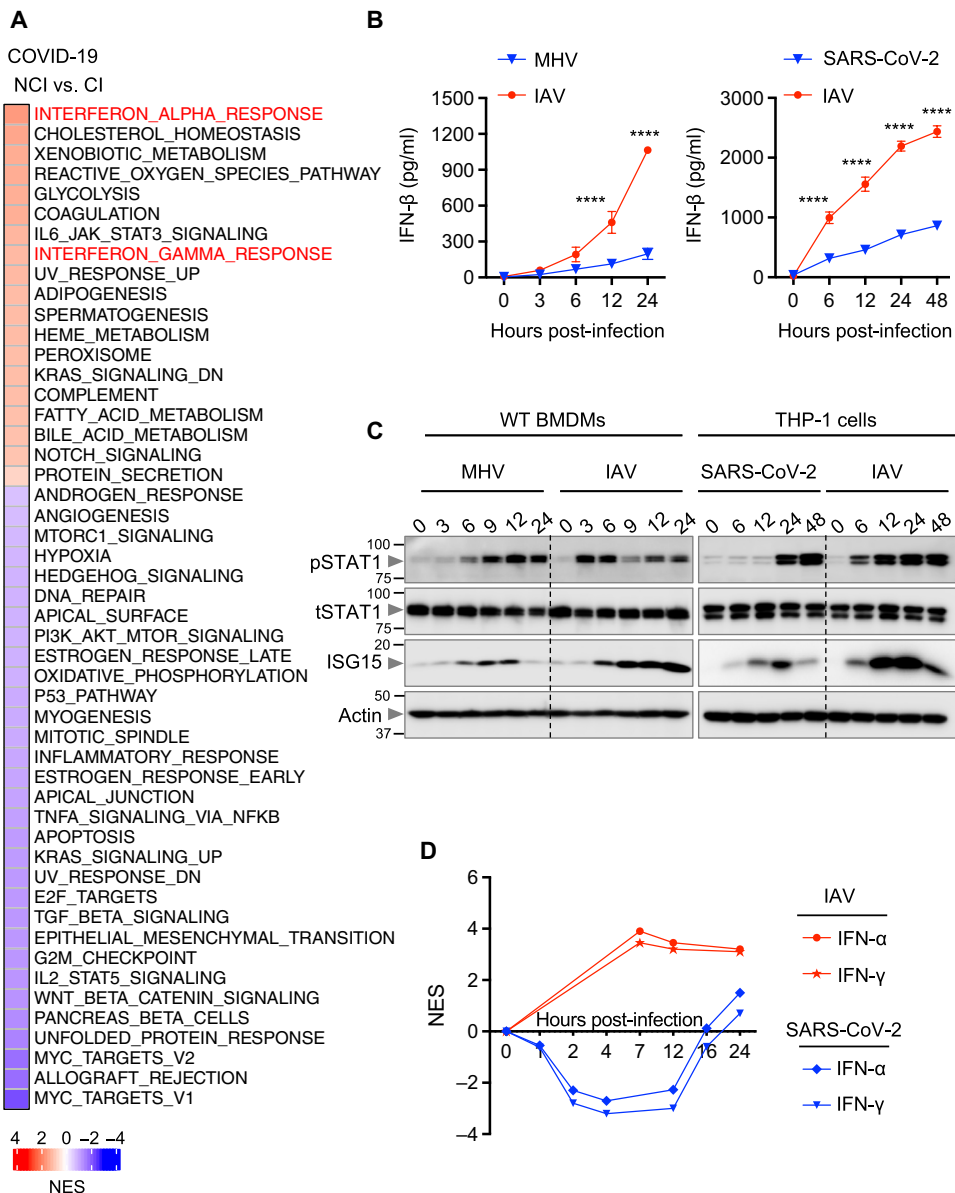
Fig. 1. Delayed IFN responses during β-coronavirus infection. (A) Heatmap depicting the altered pathways in whole blood cell transcriptomes of CI patients compared with NCI patients with COVID-19 (*35*). (**B**) IFN-β release in the supernatant of WT BMDMs infected with MHV or IAV (left) or THP-1 cells infected with SARS-CoV-2 or IAV (right) for the indicated time. (**C**) Immunoblot analysis of phosphorylated STAT1 (pSTAT1), total STAT1 (tSTAT1), and ISG15 in WT BMDMs infected with MHV or IAV (left) or THP-1 cells infected with SARS-CoV-2 or IAV (right) for the indicated time. Molecular weight marker sizes in kilodaltons are indicated in small font on the left of each blot. (**D**) Kinetics of IFN-α and IFN-γ responses in SARS-CoV-2– or IAV-infected Calu-3 cells (*42*, *43*). Data are representative of at least three independent experiments (B and C). ****$P < 0.0001$. Analysis was performed using the two-way ANOVA (B). Data are shown as means ± SEM.

septal thickening with scattered syncytial cells and extensive necrosis and loss of bronchiolar epithelium in affected areas during MHV infection (Fig. 2D and fig. S3B, arrows). The increased production of inflammatory cytokines was accompanied by an increase in alveolar, perivascular, and peribronchiolar infiltrates of immune cells, such as macrophages and neutrophils in the lungs of MHV-infected WT mice treated with IFN-β (Fig. 2D and fig. S3, C and D). In addition, there was augmented cell death, as evidenced by the presence of an increased number of TUNEL[+] (terminal deoxynucleotidyl transferase–mediated deoxyuridine triphosphate nick end labeling–positive) cells, in the lungs of MHV-infected mice treated with IFN-β compared with the infected mice treated with PBS or mock-treated mice (fig. S3, E and F), which likely accounts for the extensive necrosis and loss of bronchiolar epithelium observed in these mice. TUNEL positivity, desquamation of bronchial epithelium, marked inflammatory responses, and necrosis were also found in lung samples from human patients who succumbed to SARS-CoV-2 infection (fig. S4).
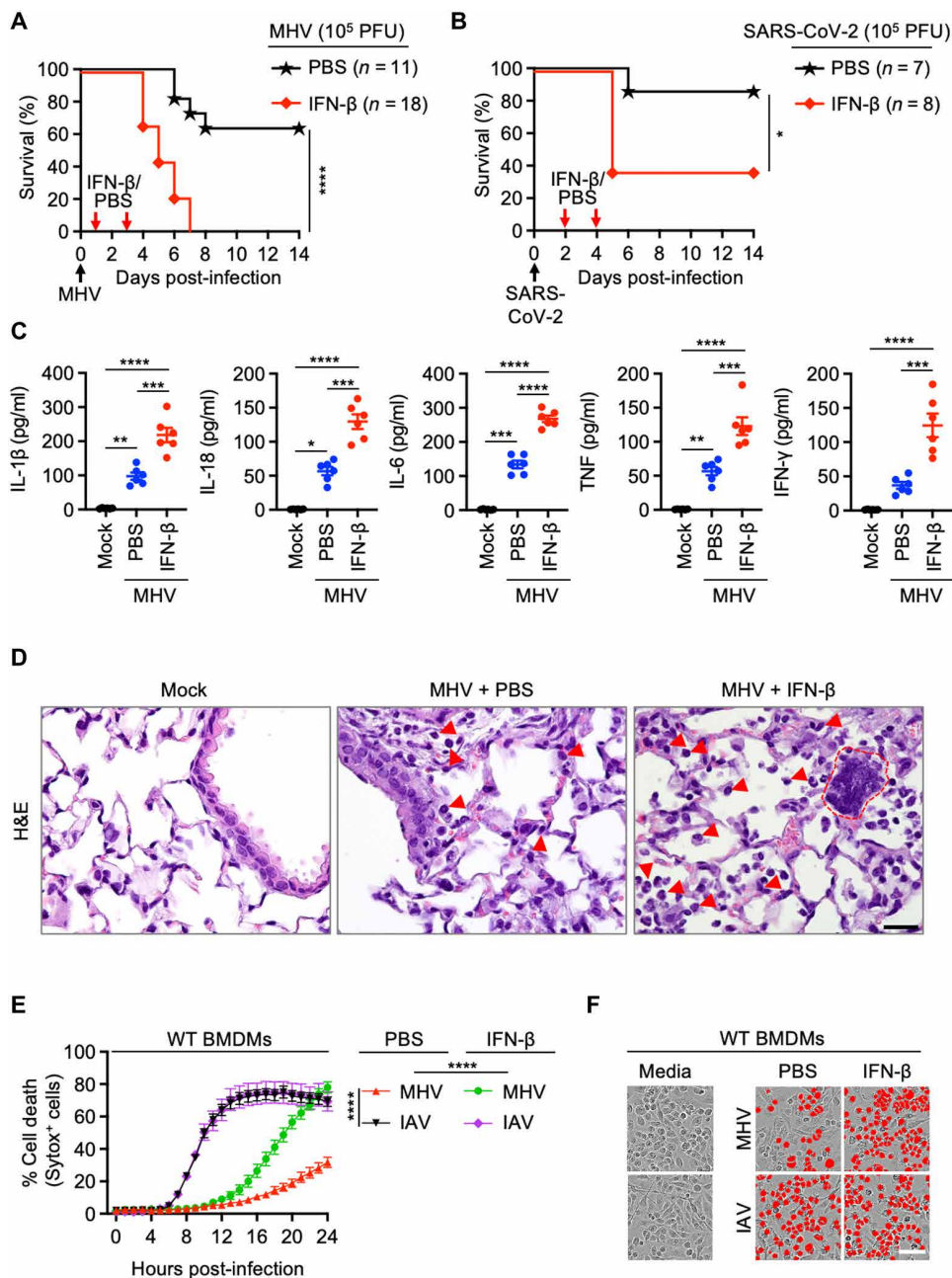
To further evaluate the molecular mechanisms of the IFN-induced pathology during infection, we tested whether the increased cell death observed in the lungs of mice treated with IFN-β during MHV infection could be recapitulated in vitro. We found that BMDMs infected with MHV showed delayed cell death compared with cells infected with IAV (Fig. 2, E and F). Moreover, treatment with IFN-β or IFN-γ, but not IL-6, IL-1β, or tumor necrosis factor (TNF), significantly increased cell death at 24 hours after MHV infection (fig. S5). Whereas addition of IFN-β after infection did accelerate MHV-induced cell death, consistent with our in vivo findings, the supplementation of IFN-β did not change the dynamics of cell death induced by IAV infection (Fig. 2, E and F). Together, these data indicate that IFN treatment robustly potentiates the ability of β-coronaviruses to induce cell death, contributing to cytokine storm, lung damage, and lethality.

IFN treatment potentiates inflammatory cell death, PANoptosis, during β-coronavirus infection
Cells may undergo multiple forms of cell death–including pyroptosis, apoptosis, necroptosis and PANoptosis–depending on the stimulus.
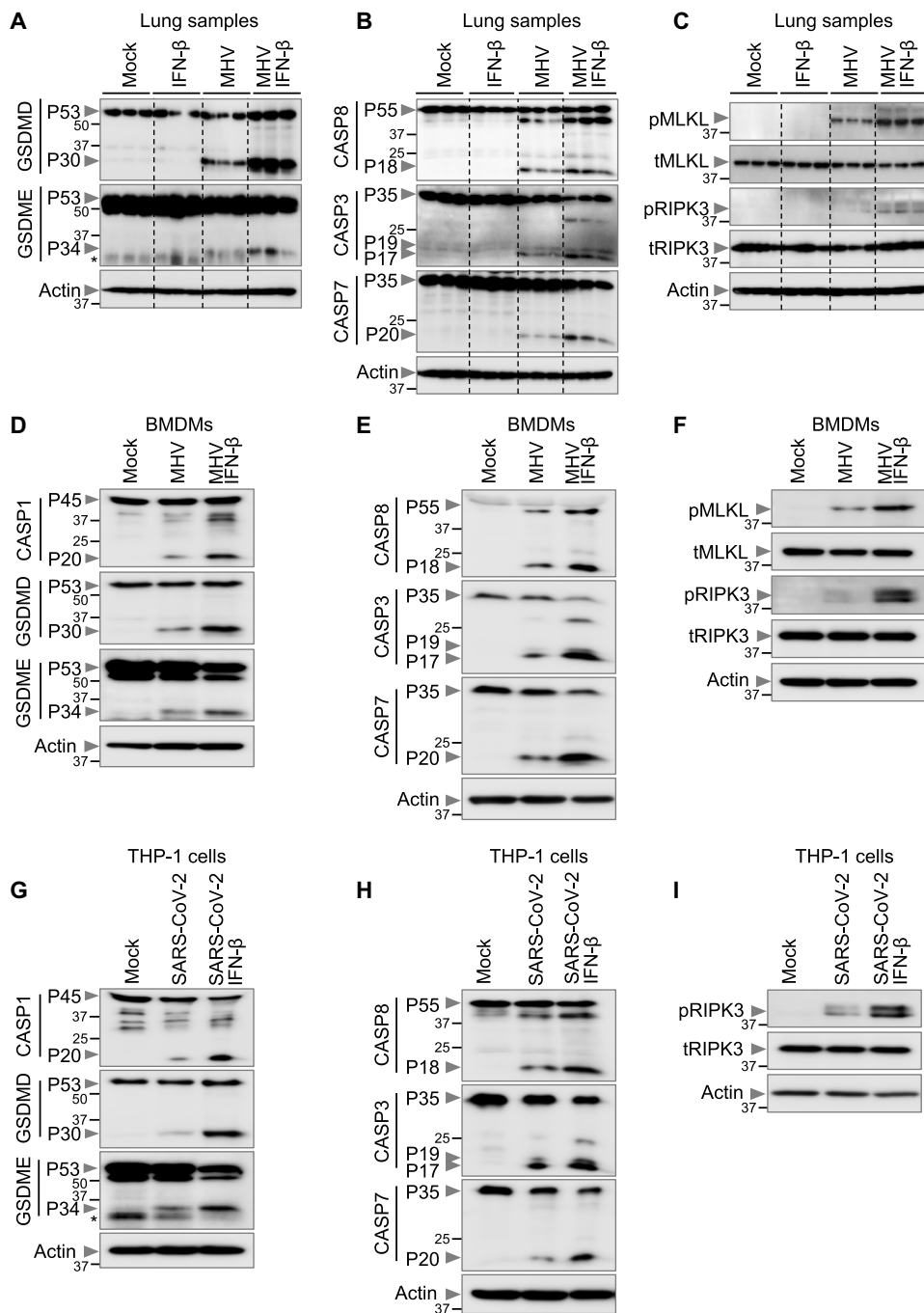
Several studies have indicated that IFNs potentiate inflammatory cell death, PANoptosis, leading to cytokine storm and organ damage (*4*, *45*). Consistent with this, at day 3 after MHV infection, we observed increased production of inflammasome-dependent cytokines interleukin-1β (IL-1β) and IL-18 as well as other pro-inflammatory cytokines in the bronchoalveolar lavage fluid (BALF) of WT mice after treatment with IFN-β compared with phosphate-buffered saline (PBS) (Fig. 2C). The lungs of IFN-β–treated mice showed widespread

Fig. 2. IFN-β treatment drives lethality, cytokine storm, and cell death during β-coronavirus infection. (**A**) Survival of 6- to 12-week-old WT mice treated with PBS (*n* = 11) or IFN-β (*n* = 18) on days 1 and 3 after intranasal infection with MHV. (**B**) Survival of 6- to 12-week-old WT mice treated with PBS (*n* = 7) or IFN-β (*n* = 8) on days 2 and 4 after intranasal infection with SARS-CoV-2. (**C**) Analysis of IL-1β, IL-18, IL-6, TNF, and IFN-γ levels in BALF of uninfected WT mice (mock, *n* = 6) or PBS-treated (*n* = 6) or IFN-β–treated (*n* = 6) WT mice 3 days after MHV infection. (**D**) H&E staining of lung samples from WT mice 3 days after MHV infection (PBS- or IFN-β–treated) or no infection (mock). Arrows indicate infiltrating immune cells, and dotted red outline represents a syncytial cell. (**E**) Real-time analysis of cell death in PBS- or IFN-β–treated WT BMDMs after infection with MHV or IAV. (**F**) Representative images of cell death in PBS- or IFN-β–treated BMDMs at 24 hours after MHV infection or 16 hours after IAV infection. Scale bars, 50 μm (D and F). Data are representative of two (A, C, and D) or at least three independent experiments (E and F). *$P < 0.05$, **$P < 0.01$, ***$P < 0.001$, and ****$P < 0.0001$. Analysis was performed using one-way ANOVA (C and E) or log-rank test (Mantel-Cox) (A and B). Each symbol represents one mouse (C). Data are shown as means ± SEM. Images are representative of an experiment containing at least five biologically independent samples in each group (D).

PANoptosis is regulated by multifaceted macromolecular complexes termed PANoptosomes (*29*, *31*, *32*, *45*, *52–66*). Previous studies have suggested that inflammatory cell death, PANoptosis, can drive cytokine storm during SARS-CoV-2 infection (*4*, *45*). Various pathogens, including bacteria, viruses, and fungi, can trigger cells to undergo PANoptosis (*31*, *53*, *54*, *56*, *61*, *63*, *66*, *67*). Therefore, the increased lethality and lung damage observed in MHV-infected mice upon IFN-β treatment could be due to robust induction of PANoptosis. We therefore biochemically characterized the activation of key PANoptotic proteins (caspase-1, GSDMD, GSDME, caspase-8, caspase-3, caspase-7, MLKL, and RIPK3) in the lungs of infected mice. We found that IFN-β treatment led to increased activation of these molecules in the lungs of WT mice infected with MHV compared with the lungs of infected mice not treated with IFN-β (Fig. 3, A to C), suggesting that IFN-β treatment potentiates PANoptosis in the lungs of the mice infected with MHV. Similarly, we observed that IFN-β treatment led to increased activation of PANoptotic molecules in BMDMs infected with MHV (Fig. 3, D to F) or THP-1 cells infected with SARS-CoV-2 (Fig. 3, G to I). Overall, these data indicate that IFN treatment potentiates inflammatory cell death, PANoptosis, that may

Mechanistically, pyroptosis is executed by gasdermin family member–mediated pore formation, which can be induced through inflammasome activation and caspase-1 cleavage of gasdermin D (GSDMD) (*46*, *47*). Apoptosis is induced by the initiator caspases caspase-8/10 or caspase-9, which activate executioners caspase-3 and caspase-7 to drive cell death (*48*, *49*). Necroptosis involves RIPK3-mediated mixed lineage kinase domain like pseudokinase (MLKL) oligomerization to induce MLKL pores in the membrane and execute cell death (*50*, *51*). Studies have recently identified another cell death pathway called PANoptosis, a unique inflammatory cell death pathway that integrates components from other cell death pathways. The totality of biological effects in PANoptosis cannot be individually accounted for by pyroptosis, apoptosis, or necroptosis alone.

Fig. 3. IFN-β promotes inflammatory cell death, PANoptosis, during β-coronavirus infection. (A to C) Immunoblot analysis of (A) pro- (P53) and activated (P30) GSDMD and pro- (P53) and activated (P34) GSDME; (B) pro- (P55) and cleaved caspase-8 (CASP8; P18), pro- (P35) and cleaved caspase-3 (CASP3; P19 and P17), and pro- (P35) and cleaved caspase-7 (CASP7; P20); and (C) phosphorylated MLKL (pMLKL), total MLKL (tMLKL), phosphorylated RIPK3 (pRIPK3), and total RIPK3 (tRIPK3) in the lung samples from mock- or IFN-β–treated WT mice with or without MHV infection 3 days after infection. **(D to I)** Immunoblot analysis of (D and G) pro- (P45) and activated (P20) caspase-1 (CASP1), pro- (P53) and activated (P30) GSDMD, and pro- (P53) and activated (P34) GSDME; (E and H) pro- (P55) and cleaved CASP8 (P18), pro- (P35) and cleaved CASP3 (P19 and P17), and pro- (P35) and cleaved CASP7 (P20); (F) pMLKL, tMLKL, pRIPK3, and tRIPK3; and (I) pRIPK3 and tRIPK3 in mock- or IFN-β–treated BMDMs or THP-1 cells during MHV or SARS-CoV-2 infection, respectively. Actin was used as the internal control. Molecular weight marker sizes in kilodaltons are indicated in small font on the left of each blot. Asterisk denotes nonspecific bands (A and G). Data are representative of at least three independent experiments.

drive cytokine storm, pathology, and lethality in the mice during β-coronavirus infection.

ZBP1 contributes to pathology and lethality during β-coronavirus infection

Cytosolic sensors that are involved in sensing and inducing inflammatory cell death during β-coronavirus infection remain largely unknown. To identify the innate immune sensors that are required for cell death during β-coronavirus infection, we performed a whole-genome CRISPR-CAS9 KO screen in murine immortalized BMDMs (iBMDMs) using MHV. After generating a pool of cells with individual genes deleted by CRISPR, we infected them with MHV for 24 hours and analyzed the surviving pool of cells to identify the genes that were enriched or depleted in this population. The enriched genes in the surviving pool of cells could be potentially important to play a positive role in inducing cell death during β-coronavirus infection. Because IFN-β treatment contributed to lethality in mice, we then focused our analysis on the ISGs that were significantly up-regulated in the surviving pool (Fig. 4A and table S1). Of these ISGs, ZBP1 has been reported to trigger inflammatory cell death in several contexts (*29, 31, 34, 53, 66, 68*), including viral infection with IAV. Moreover, *ZBP1* was also identified among the ISGs up-regulated in CI patients with COVID-19 (fig. S1B). Therefore, we hypothesized that ZBP1 may be involved in lethality observed in patients with severe COVID-19. To further explore whether ZBP1 expression may correlate with pathology, we reanalyzed publicly available single-cell RNA-seq datasets to examine the expression of *ZBP1* in immune cells from healthy patients compared with cells from patients with stable COVID-19, who did not require hospitalization, and with cells from those with progressive COVID-19, which led to lethality (*69*). We observed that the expression of *ZBP1* was significantly increased in neutrophils, dendritic cells, macrophages, basophils, natural killer (NK) cells, CD4$^+$ T cells, and regulatory T (T$_{reg}$) cells from patients with COVID-19 compared with healthy controls (fig. S6A). Moreover, patients with progressive COVID-19, who succumbed to infection, had increased *ZBP1* expression
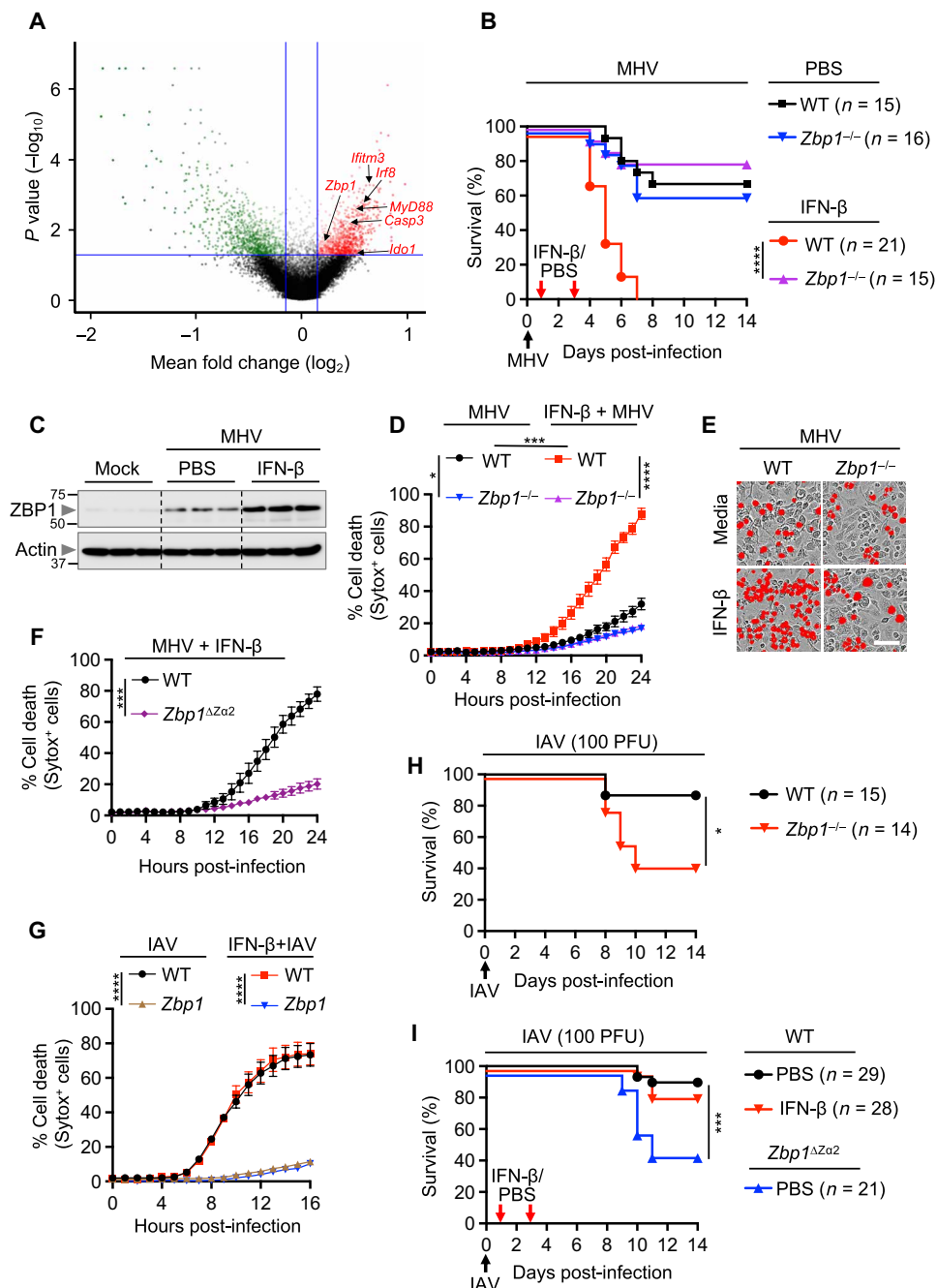
Fig. 4. IFN-β–driven lethality, cytokine storm, and cell death depend on ZBP1 during β-coronavirus infection. (**A**) Volcano plot showing the genes that are enriched or depleted in iBMDMs after a genome-wide CRISPR-CAS9 KO screen of cell death induced by MHV infection (MOI 0.2, 24 hours). (**B**) Survival of 6- to 12-week-old WT and *Zbp1⁻/⁻* mice treated with PBS (*n* = 15 for WT and *n* = 16 for *Zbp1⁻/⁻* mice) or IFN-β (*n* = 21 for WT and *n* = 15 for *Zbp1⁻/⁻* mice) on days 1 and 3 after intranasal infection with MHV. (**C**) Immunoblot analysis of ZBP1 in the lung samples from PBS- or IFN-β–treated WT mice 3 days after MHV infection. Molecular weight marker sizes in kilodaltons are indicated in small font on the left of each blot. Actin was used as the internal control. (**D**) Real-time analysis of cell death in MHV-infected WT or *Zbp1⁻/⁻* BMDMs in the presence or absence of IFN-β. (**E**) Representative images of cell death in media- or IFN-β–treated WT or *Zbp1⁻/⁻* BMDMs are shown at 24 hours after MHV infection. Scale bar, 50 μm. (**F**) Real-time analysis of cell death in MHV-infected WT or *Zbp1^ΔZα2* BMDMs in the presence of IFN-β. (**G**) Real-time analysis of cell death in IAV-infected WT or *Zbp1⁻/⁻* BMDMs in the presence and absence of IFN-β. (**H**) Survival of 6- to 12-week-old WT (*n* = 15) and *Zbp1⁻/⁻* (*n* = 14) mice after intranasal infection of IAV. (**I**) Survival of 6- to 12-week-old WT and *Zbp1^ΔZα2* mice treated with PBS (*n* = 29 for WT and *n* = 21 for *Zbp1^ΔZα2* mice) or IFN-β (*n* = 28 for WT mice) on days 1 and 3 after intranasal infection of IAV. Survival data are pooled from two infection experiments (B, H, and I). All other data are representative of at least three independent experiments. *$P < 0.05$, ***$P < 0.001$, and ****$P < 0.0001$. Analysis was performed using the one-way ANOVA (D and G), two-tailed *t* test (F), or log-rank test (Mantel-Cox) (B, H, and I). Data are shown as means ± SEM.

in their immune cells, particularly NK cells, CD4⁺ memory and naïve T cells, effector memory CD8⁺ T cells, and B memory and naïve cells, compared with patients with stable COVID-19 (fig. S6B). Together, these data suggest a positive correlation between *ZBP1* expression and disease and lethality in patients with COVID-19.

Next, we sought to determine the physiological role of ZBP1 in driving lethality and cell death during β-coronavirus infection in the presence or absence of IFN-β treatment. Although IFN-β treatment substantially increased the lethality of MHV infection in WT mice, mice that were deficient in ZBP1 were similarly susceptible to MHV infection–induced lethality whether or not they received

inflammasome-dependent and inflammasome-independent proinflammatory cytokines in the BALF of MHV-infected *Zbp1⁻/⁻* mice compared with those of WT mice after IFN-β treatment (fig. S7). The regulatory role of ZBP1 in vivo was further confirmed by in vitro findings that the robust cell death observed in MHV-infected BMDMs in response to IFN treatment was reduced in ZBP1-deficient cells (Fig. 4, D and E). Sensing of viral or endogenous Z-RNA by the Zα domains of ZBP1 triggers NLRP3 inflammasome activation, inflammatory cell death, and perinatal lethality in mice, indicating that the Zα domains are crucial to regulate the immune responses driven by ZBP1 (*32–34*). Therefore, we investigated the role of the Zα2 domain of ZBP1 in driving the cell death induced by MHV

IFN-β treatment (Fig. 4B). We found that ZBP1 expression was greatly enhanced in the lungs of MHV-infected mice after IFN-β treatment compared with the lungs of untreated infected mice (Fig. 4C). Moreover, we observed decreased production of inflammasome-dependent and inflammasome-independent pro-

with IFN-β treatment. Similar to *Zbp1*⁻/⁻ BMDMs, MHV-infected cells lacking the Zα2 domain of ZBP1 showed reduced cell death compared with those of WT BMDMs after treatment with IFN-β (Fig. 4F). However, IFN-β treatment did not affect the ZBP1-dependent cell death in BMDMs during IAV infection (Fig. 4G), likely because IAV infection naturally induces more rapid IFN production than β-coronavirus infection, making the additional IFN ineffective. Although *Zbp1*⁻/⁻ and *Zbp1*^ΔZα2 mice showed increased susceptibility to IAV infection with respect to WT mice, IFN-β treatment did not change the outcome in WT mice during IAV infection (Fig. 4, H and I). Together, our results show that ZBP1 drives cell death, cytokine storm, and lethality in β-coronavirus–infected mice in response to IFN-β treatment.

ZBP1 triggers inflammatory cell death, PANoptosis, and cytokine storm during β-coronavirus infection

ZBP1 has been shown to trigger cell death by activating PANoptosis in cells during infection with viruses and fungi (*31, 32, 53, 63, 66*). Combined with our observation that PANoptosis was occurring in the lungs of MHV-infected mice in response to IFN-β treatment (Fig. 3, A to C), this suggests that ZBP1-mediated PANoptosis may contribute to lung pathology, cytokine storms, and lethality in MHV-infected mice during IFN-β treatment. In support of this hypothesis, we found that the robust activation of PANoptotic markers was reduced in the lungs of MHV-infected *Zbp1*⁻/⁻ mice compared with those of WT mice during IFN-β treatment (Fig. 5, A to C). In addition, consistent with the reduced cell death observed in *Zbp1*⁻/⁻ and *Zbp1*^ΔZα2 BMDMs (Fig. 4, D to F), these cells also showed impaired activation of PANoptotic effectors in response to IFN-β treatment (Fig. 5, D to F). Similarly, *ZBP1*-silenced THP-1 cells infected with SARS-CoV-2 showed reduced activation of PANoptotic effectors when treated with IFN-β compared with control-infected and IFN-β–treated cells (fig. S8, A and B). Together, these results indicate that ZBP1, and specifically its Zα2 domain, is required for β-coronavirus–induced inflammatory cell death in response to IFN-β treatment.

ZBP1 activation leads to its interaction with RIPK3 and recruitment of caspase-8 and caspase-6 to form a cell death signaling scaffold, termed the ZBP1-PANoptosome, that drives NLRP3 inflammasome activation and cell death (*31, 32, 63, 70*). We therefore assessed whether RIPK3 and caspase-8 had any role in the β-coronavirus–induced cell
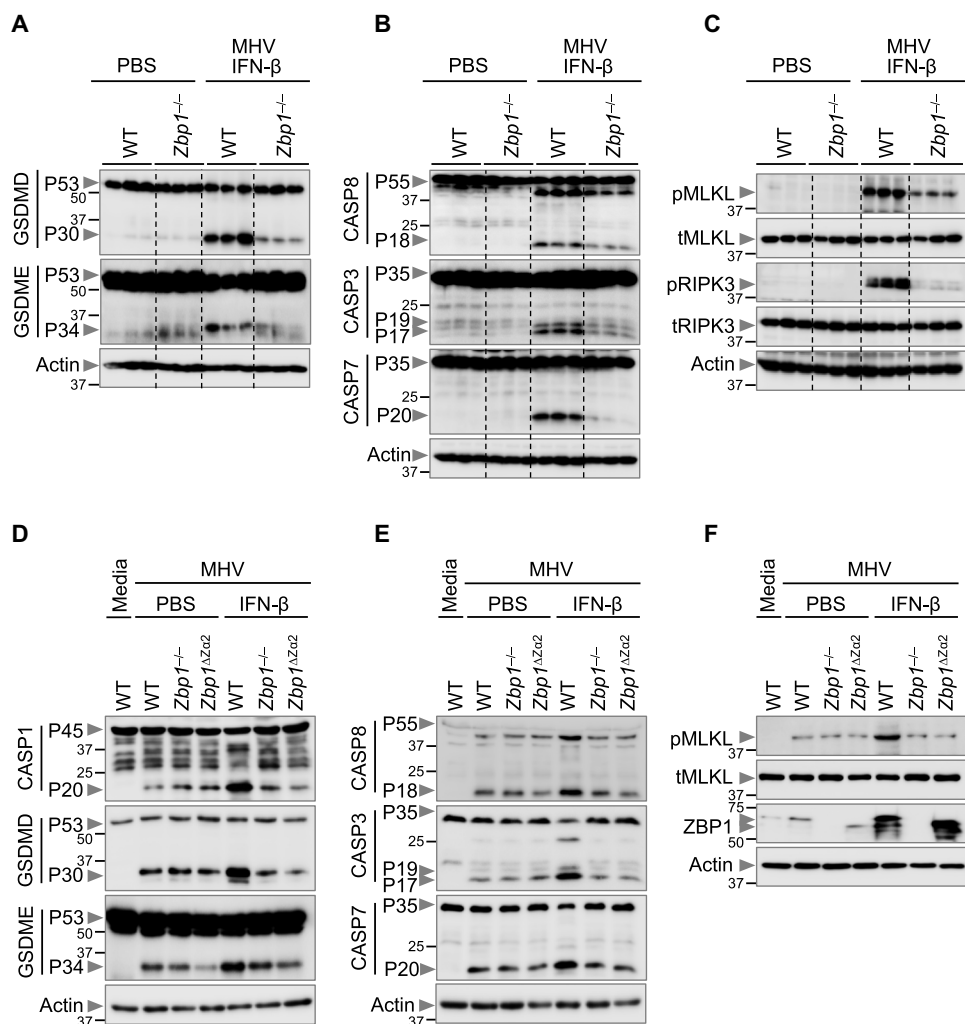
Fig. 5. Zα domain of ZBP1 drives PANoptosis mediated by IFN-β during β-coronavirus infection. (**A** to **C**) Immunoblot analysis of (A) pro- (P53) and activated (P30) GSDMD and pro- (P53) and activated (P34) GSDME; (B) pro- (P55) and cleaved (P18) CASP8, pro- (P35) and cleaved (P19 and P17) CASP3, and pro- (P35) and cleaved (P20) CASP7; and (C) pMLKL, tMLKL, pRIPK3, and tRIPK3 in the lung samples from WT and *Zbp1*⁻/⁻ mice that were PBS-treated or MHV-infected and treated with IFN-β, then harvested 3 days after infection. (**D** to **F**) Immunoblot analysis of (D) pro- (P45) and activated (P20) CASP1, pro- (P53) and activated (P30) GSDMD, and pro- (P53) and activated (P34) GSDME; (E) pro- (P55) and cleaved (P18) CASP8, pro- (P35) and cleaved (P19 and P17) CASP3, and pro- (P35) and cleaved (P20) CASP7; and (F) pMLKL, tMLKL, and ZBP1 in PBS- or IFN-β–treated WT, *Zbp1*⁻/⁻, and *Zbp1*^ΔZα2 BMDMs during MHV infection. Actin was used as the internal control. Data are representative of at least three independent experiments.

death pathway during IFN-β treatment. Similar to *Zbp1*⁻/⁻ or *Zbp1*^ΔZα2 BMDMs, cells lacking RIPK3 showed reduced cell death and activation of PANoptotic molecules compared with those of WT BMDMs during MHV infection in response to IFN-β treatment (fig. S8, C to G). We did not observe significant differences in the extent of cell death and activation of PANoptosis between *Ripk3*⁻/⁻ and *Ripk3*⁻/⁻*Casp8*⁻/⁻ BMDMs (fig. S8, C to G), indicating that the phenotype observed in *Ripk3*⁻/⁻*Casp8*⁻/⁻ BMDMs is largely attributed to the RIPK3 deficiency because caspase-8 is upstream of RIPK3. Together, these findings suggest that ZBP1-mediated activation of RIPK3-dependent PANoptosis is responsible for the cell death induced by IFN-β treatment during β-coronavirus infection.

DISCUSSION

Vaccines remain the best approach to end the COVID-19 pandemic (71). However, the efficacy of the vaccines is challenged by the emergence of new SARS-CoV-2 variants (72). Use of drugs—including the antivirals remdesivir, the nirmatrelvir and ritonavir combination (Paxlovid), and molnupiravir, as well as anti-inflammatory or immunomodulatory agents such as dexamethasone, tocilizumab, and baricitinib—has been shown to improve outcomes in patients with COVID-19 (73–77). However, these agents typically provide limited benefits to a subset of patients, and global availability is inadequate; the morbidity and mortality caused by COVID-19 remain high (1). Given the potency of IFNs in controlling viral replication, several clinical trials using IFNs alone or in combination with other antiviral drugs have been initiated to treat patients infected with SARS-CoV-2. Coronaviruses, including SARS-CoV-2 and MHV, induce a delayed IFN response (18, 19), because of which the viruses likely undergo active replication to establish infection. However, preclinical data have shown that this delayed response can be overcome by treatment with exogenous IFNs or IFN-inducing agonists (19). The observed benefits of early type I IFN responses induced by some agonists in preclinical models suggest that IFN-based therapies may be effective for the prevention and treatment of COVID-19 (19–23, 78, 79). However, the use of IFN therapy, which acts by decreasing viral replication, has shown mixed responses in clinical trials (24, 25, 80–85). A recent double-blinded and placebo-controlled clinical trial (ACTT-3) showed no significant difference in patient outcomes with the combination of IFN-β-1a plus remdesivir compared with remdesivir alone, suggesting no clinical benefits of IFN therapy in patients with COVID-19 (24). Moreover, patients who required supplemental oxygen or noninvasive ventilation tended to develop adverse outcomes, particularly worsening respiratory function, in response to IFN-β-1a administration in this trial (24). It is possible that IFN treatment may increase the inflammatory response, leading to more severe respiratory disease in these patients.

In vivo, the lungs of MHV-infected mice had increased immune cell infiltration, inflammatory cytokine levels, and PANoptosis in response to IFN treatment compared with PBS treatment, and the IFN-treated mice were more likely to succumb to infection. Similar survival was observed in SARS-CoV-2–infected mice, where IFN treatment significantly increased mortality. In vitro, MHV-infected BMDMs or SARS-CoV-2–infected monocytes showed increased PANoptosis after IFN treatment compared with mock treatment. BMDMs or THP-1 cells were treated with IFN-β after 5 hours of MHV or SARS-CoV-2 infection. However, the effect of IFN-β treatment at different time points after β-coronavirus infection has not been investigated in this study, and the outcomes may change depending on when IFN-β treatment is given. Moreover, the dose of IFN-β is another factor that may influence the outcome. In addition, because epithelial cells are the primary cells that are infected by β-coronaviruses, future work to determine the activation of PANoptosis in cell types other than myeloid cells, such as epithelial and endothelial cells, would provide additional information about the cell types that respond to IFNs and are responsible for driving detrimental effects during β-coronavirus infections. In addition, PANoptosis in macrophages activates both GSDMD and GSDME pore-forming molecules during SARS-CoV-2 infection, but it is possible that these molecules may have PANoptosis-independent functions in certain cell types. For instance, high expression of GSDMD has been associated with neutrophil extracellular trap (NET) structures in the lungs of patients with

COVID-19. Pharmacological inhibition of GSDMD through treatment with the inhibitor disulfiram reduces NET release and organ damage in a mouse model of SARS-CoV-2 infection, suggesting that GSDMD-dependent NETosis plays a critical role in COVID-19 immunopathology (86). These functions require further study.

IFNs, particularly IFN-γ, synergize with TNF to induce inflammatory cell death, leading to organ and tissue damage in cytokine storm–associated mouse models (4, 45). Moreover, IFNs can damage the lung epithelial barrier and impair lung epithelial regeneration during viral infection (87). In addition, IFN treatment induces sustained expression of ISGs (19), which include both antiviral and inflammatory cell death–driving molecules, such as ZBP1. Not all patients infected with SARS-CoV-2 showed increased IFN responses and ZBP1 expression. However, we observed that CI patients with more severe COVID-19 showed increased IFN responses and ZBP1 expression compared with noncritical patients with COVID-19, suggesting that IFNs and ZBP1 are associated with disease progression and mortality. The loss of ZBP1 substantially protected the β-coronavirus–infected mice from lung damage, cytokine storm, and lethality during IFN treatment, highlighting the detrimental effect of ZBP1 in disease progression. The use of IFN therapy in patients infected with SARS-CoV-2 would therefore likely mimic the increased and sustained ZBP1 expression observed in CI patients with COVID-19, which could result in multiorgan damage, cytokine storm, and mortality in patients. In contrast to its role in response to IFN treatment during β-coronavirus infection, we observed that ZBP1 was critical to the host defense against IAV infection irrespective of IFN treatment. This is likely due to the ability of IAV to induce rapid IFN responses and ZBP1 expression, which facilitates viral clearance via molecular mechanisms that include ZBP1-dependent inflammatory cell death (31, 88, 89). However, in addition to clearing the virus, dysregulated inflammatory cell death leads to cytokine storm and organ damage (4, 45). MHV-infected mice succumbed to infection upon IFN treatment despite the fact that IFN should inhibit viral replication, suggesting that inflammatory cell death, rather than the virus, is responsible for driving pathological effects. However, these consequential pathological effects of IFN therapy during β-coronavirus infection can be blocked by inhibiting ZBP1 activity. Therefore, inhibiting ZBP1 activity may improve the beneficial effects of IFN-β therapy during β-coronavirus infection. Moreover, the associated side effects and inconvenience associated with exogenous IFN administration can be overcome by administering agonists that engage DNA sensing pathways, such as cGAS and STING, or RNA sensing pathways, such as MDA5, RIG-I, and MAVS, to produce IFNs endogenously (19–22). The sustained and late IFN production induced by the cGAS-STING pathway also contributes to collateral host responses and tissue damage leading to lethality in SARS-CoV-2–infected mice (90), which could be due to ZBP1-dependent inflammatory cell death, and these factors would need to be considered when designing therapeutic strategies.

Overall, our results suggest that IFN-based treatments for COVID-19 face therapeutic challenges due to ZBP1-mediated inflammatory cell death that contributes to cytokine storm, tissue damage, and, ultimately, lethality. Combination strategies that block ZBP1 while also providing IFN treatment may therefore be beneficial for patient outcomes and should be pursued for further research and development. This improved understanding of the mechanistic basis of innate immune sensing, IFN-mediated pathology, and inflammatory cell death during SARS-CoV-2 infection informs COVID-19

therapeutic development and provides fundamental molecular details that should be evaluated across interferonopathies.

MATERIALS AND METHODS
Study design
The aim of this study was to investigate the molecular mechanism underlying the failure of IFN therapy during SARS-CoV-2 infection. We used MHV, a prototypical virus of the β-coronavirus genus that mimics many of the key aspects of human β-coronavirus biology, as well as SARS-CoV-2 to infect WT mice in the presence and absence of IFN-β and determined pathology and lethality. We also performed a CRISPR screen to identify key molecules involved in cell death in response to MHV infection. Furthermore, we investigated the effect of IFN treatment on mouse BMDMs infected with MHV and human THP-1 cells infected with SARS-CoV-2 in inducing inflammatory cell death, PANoptosis. Sample sizes used in each experiment are detailed in the figure legends.

Mice
C57BL/6J (WT), $Zbp1^{-/-}$ (91), $Zbp1^{\Delta Z\alpha2/\Delta Z\alpha2}$ (32), $Ripk3^{-/-}$ (92), and $Ripk3^{-/-}Casp8^{-/-}$ (93) mice have been described previously. All mice were bred and maintained in a specific pathogen–free facility at the Animal Resources Center at St. Jude Children's Research Hospital and were backcrossed to the C57BL/6 background (J substrain) for at least 10 generations. Both male and female mice were used in this study; 6- to 12-week-old age- and sex-matched mice were used for in vivo and in vitro studies and were randomly assigned to different treatment groups/stimulations. Cohoused animals were used for in vivo MHV infections. Mice were maintained with a 12-hour light/dark cycle and were fed standard chow. Animal studies were conducted under protocols approved by the St. Jude Children's Research Hospital committee on the Use and Care of Animals or with the approval of the Institutional Animal Care and Use Committee of University of Tennessee Health Science Center (UTHSC IACUC; protocol #20-0132).

Cell culture
Primary BMDMs from mice were cultivated for 6 days in Iscove's modified Dulbecco's medium (IMDM) (Thermo Fisher Scientific, 12440061) supplemented with 10% fetal bovine serum (FBS) (Biowest, S1620), 30% L929-conditioned media, 1% nonessential amino acids (Thermo Fisher Scientific, 11140-050), and 1% penicillin-streptomycin (Thermo Fisher Scientific, 15070-063). BMDMs were then seeded into 12-well plates at a density of 1 million cells per well and incubated overnight before use. THP-1 cells were grown in RPMI 1640 with 10% FBS and differentiated into macrophages in RPMI 1640 medium containing 20% FBS and phorbol 12-myristate 13-acetate (PMA; 100 ng/ml) for 2 days.

Virus culture
The MHV (A59 strain from R. Channappanavar) (94) was amplified in 17Cl-1 cells as previously described (95). Briefly, 17Cl-1 cells were inoculated with MHV-A59 at a multiplicity of infection (MOI) of 0.1. At 48 hours after infection, the whole flask with media and cells was frozen at −80°C and then thawed at 37°C. After repeating the freezing-thawing cycle twice, the supernatant was collected and centrifuged at 2000g for 10 min to remove the cell debris. Then, the virus was purified by ultracentrifugation at 30,000 rpm for 1 hour, after which the pellets were resuspended with fresh medium. The virus titer was measured by plaque assay in 17Cl-1 cells. SARS-CoV-2 for in vitro analyses (strain USA-WA1/2020 isolate; BEI Resources, catalog no. NR-52281) was obtained from BEI Resources (www.beiresources.org) and amplified in Vero E6 cells. SARS-CoV-2 for in vivo analyses (isolate hCoV-19/USA/MD-HP01542/2021; lineage B.1.351, NR-55282) was obtained from BEI Resources. SARS-CoV-2 B.1.351 (Beta) seed stocks were amplified in Vero E6/TMPRSS2 cells in infection media comprising minimum essential medium with Earle's salts and L-glutamine with 2% FBS and 1% penicillin-streptomycin. Amplified stock virus was stored at −80°C until used. The IAV (A/Puerto Rico/8/34, H1N1 [PR8]) was prepared as previously described (63) and propagated from 11-day-old embryonated chicken eggs by allantoic inoculation. IAV titer was measured by plaque assay in Madin-Darby canine kidney (MDCK) cells.

Cell stimulation and infection
For MHV (16 or 24 hours; MOI 0.5, unless otherwise noted) and IAV (16 hours; MOI 5, unless otherwise noted) infections, cells were infected in Dulbecco's modified Eagle's medium (DMEM) plain media without glutamic acid and sodium pyruvate (Sigma-Aldrich, D6171). For SARS-CoV-2 infection, THP-1 cells were seeded in six-well plates and activated with PMA (10 ng/ml) for 2 to 3 days. THP-1 cells were infected by incubating with SARS-CoV-2 (MOI 0.1 for 1 hour) in a CO_2 incubator at 37°C. After, cells were washed once with PBS and replenished with media. Infected cells were then cultured in a CO_2 incubator at 37°C. For cytokine treatment, BMDMs were stimulated with the following concentrations of cytokines: IL-6 (20 ng/ml; PeproTech, 212-16), IL-1β (20 ng/ml; R&D Systems, 201-LB-025), TNF (25 ng/ml; PeproTech, 315-01A), IFN-γ (50 ng/ml; PeproTech, 315-05), or IFN-β (50 ng/ml; PBL Assay, 12400-1) for the indicated time. Human THP-1 macrophages were stimulated with IFN-β (50 ng/ml; PBL Assay, 11410-2) for the indicated time. Cytokines were added to BMDMs or THP-1 cells 5 hours after infections.

siRNA-mediated gene silencing
The Accell human small interfering RNAs (siRNAs) against $ZBP1$ (E-014650-00-0010) were purchased (Horizon). THP-1 macrophages were transfected with siRNA using Accell siRNA delivery media according to the manufacturer's instructions (Horizon). As a negative control, nontargeting control siRNA (D-001910-01-50) was used.

In vivo infection
Six- to 12-week-old age- and sex-matched WT, $Zbp1^{-/-}$, and $Zbp1^{\Delta Z\alpha2/\Delta Z\alpha2}$ mice were used for infections. Mice were anesthetized with Avertin (250 mg/kg) and then infected intranasally. For determination of the LD_{50} dose of MHV, mice were infected with 50 μl of PBS containing ~10^4, ~10^5, or ~10^6 plaque-forming units (PFU) of MHV. For subsequent infections, mice were infected with 50 μl of PBS containing ~10^5 PFU of MHV or ~100 PFU of IAV. The MHV-infected mice were injected intraperitoneally with 200 μl of PBS or IFN-β (1 μg/mouse) diluted in PBS on days 1 and 3 after infection. The mice were monitored over a period of 14 days for survival. For collection of BALF or lungs, mice were dosed with PBS or IFN-β as described above on day 1, and samples were collected at day 3 after infection.

SARS-CoV-2 infections were conducted in accordance with the approval of the UTHSC IACUC (protocol #20-0132). The SARS-CoV-2–related experiments were performed in animal biosafety

level 3 conditions within the UTHSC Regional Biocontainment Laboratory (RBL) according to UTHSC RBL Standard Operating Procedures and safety manuals. Each mouse was intranasally infected with SARS-CoV-2 B.1.351 variant at 1×10^5 PFU in a total volume of 100 μl (50 μl per nare) at day 0. The SARS-CoV-2–infected mice were injected intraperitoneally with 150 μl of PBS or IFN-β (1 μg per mouse) diluted in PBS on days 2 and 4 after infection. Mice were weighed and monitored daily in the morning. The mice health status was evaluated once per day using the clinical scoring system approved by UTHSC IACUC, then twice daily upon clinical manifestation. The mice were monitored over a period of 14 days for survival.

Histopathology

For murine samples, lungs were fixed in 10% formalin and then processed and embedded in paraffin by standard procedures. Sections (5 μm) were stained with hematoxylin and eosin (H&E) and examined by a pathologist blinded to the experimental groups. For immunohistochemistry, formalin-fixed paraffin-embedded lungs were cut into 4-μm sections. F4/80 [Cell Signaling Technology (CST), D2SR9] and Ly-6B.2 (Novus, NBP2-13077) staining was performed according to the manufacturer's instructions. TUNEL staining was performed using the Dead-End Kit (Promega, PRG7130) according to the manufacturer's instructions.

For human lung samples, deidentified autopsy lung samples were provided by the Asian Institute of Gastroenterology as paraffin-embedded tissue blocks. Sectioning (4 μm) and immunohistochemistry were performed by HistoWiz with H&E, the rabbit polyclonal anti–SARS-CoV-2 nucleocapsid (N) protein antibody (GeneTex; GTX635686), and TUNEL (Promega) staining following standard protocols.

Immunoblot analysis

Immunoblotting was performed as described previously (96). Briefly, for caspase analysis, BMDMs were lysed along with the supernatant using 50 μl of caspase lysis buffer (1× protease inhibitors, 1× phosphatase inhibitors, 10% NP-40, and 25 mM dithiothreitol) followed by the addition of 100 μl of 4× SDS loading buffer. For signaling analysis, the BMDM supernatants were removed at the indicated time points, and cells were washed once with PBS, after which cells were lysed with radioimmunoprecipitation assay (RIPA) buffer. Proteins from lung tissues were extracted using RIPA buffer supplemented with protease and phosphatase inhibitors (Roche), and 30 μg per sample was loaded on the gel. Proteins were separated by electrophoresis through 8 to 12% polyacrylamide gels. After electrophoretic transfer of proteins onto polyvinylidene difluoride membranes (Millipore, IPVH00010), nonspecific binding was blocked by incubation with 5% skim milk; then, membranes were incubated with the following primary antibodies: anti–caspase-1 (1:1000; AdipoGen, AG-20B-0042), anti–caspase-3 (1:1000; CST, #9662), anti–cleaved caspase-3 (1:1000; CST, #9661), anti–caspase-7 (1:1000; CST, #9492), anti–cleaved caspase-7 (1:1000; CST, #9491), anti–caspase-8 (1:1000; CST, #4927), anti–cleaved caspase-8 (1:1000; CST, #8592), anti–phosphorylated RIPK3 (1:1000; CST, #91702S), anti-RIPK3 (1:1000; ProSci, #2283), anti–phosphorylated MLKL (1:1000; CST, #37333), anti-MLKL (1:1000; Abgent, AP14272b), anti-GSDMD (1:1000; Abcam, ab209845), anti-GSDME (1:1000; Abcam, ab215191), anti–phosphorylated STAT1 (1:1000; CST, #7649), anti-STAT1 (1:1000; CST, #14994), anti-ZBP1 (1:1000; AdipoGen, AG-20B-0010, 1:1000), anti–β-actin (1:5000; Proteintech, 66009-1-IG), human

anti–caspase-1 (1:1000; R&D Systems, catalog no. MAB6215), human anti–caspase-8 (1:1000; Enzo, ALX-804-242), human anti-GSDMD (1:1000; Abcam, ab210070, 1:1000), human anti–total MLKL (1:1000; Abcam, ab184718), human anti–β-actin (1:1000; CST, 4970) and anti-ISG15 (Santa Cruz Biotechnology, sc-166755). Membranes were then washed and incubated with the appropriate horseradish peroxidase (HRP)–conjugated secondary antibodies [1:5000 dilution; Jackson ImmunoResearch Laboratories, anti-rabbit (111-035-047), anti-mouse (315-035-047)] for 1 hour. Proteins were visualized by using Luminata Forte Western HRP Substrate (Millipore, WBLUF0500), and membranes were developed with an Amersham imager.

Real-time cell death analysis

Real-time cell death assays were performed using an IncuCyte S3 or IncuCyte SX5 imaging system (Sartorius). BMDMs were seeded in 12-well plates (10^6 cells per well) and stimulated. After infection, 100 nM Sytox Green (Thermo Fisher Scientific, S7020) was added. The images were acquired every 1 hour at 37°C and 5% CO_2. The resulting images were analyzed using the software package supplied with the IncuCyte imager, which counts the number of Sytox Green–positive BMDM nuclei (Sytox$^+$ BMDM nuclei) present in each image.

Cytokine analysis

Cytokines were detected by using multiplex enzyme-linked immunosorbent assay (ELISA) (Millipore, MCYTOMAG-70K) or IL-18 ELISA (Invitrogen, BMS618-3) according to the manufacturer's instructions.

Microarray and RNA-seq analysis

For analysis of gene expression in patients with COVID-19, publicly available datasets were downloaded from the Gene Expression Omnibus (GEO) database [GSE147507 (18), GSE171430 (97), GSE157103 (98), and GSE171110 (99)]. The DESeq2 v1.32.0 (100) package was used to read the count matrices and remove genes that were not expressed in at least one sample, and the limma v3.48.3 package (101) in R v4.1.1 was used to determine differential expression. Benjamini-Hochberg (102) adjusted P value < 0.05 and |log2FC| > 1 were then used to identify the differentially expressed genes. Genes that were differentially expressed in each of the four datasets were then used to form a consensus set of 31 genes consistently expressed differentially and with significance across the four COVID-19–related datasets. This gene set was used for subsequent analyses.

Unnormalized RNA-seq data were obtained from BioProject [PRJNA638753 (35)] to compare NCI with CI patients with COVID-19. Quality control steps were performed, including normalizing quantiles using the "normalize.quantiles" function from the preprocessCore v1.54.0 package, followed by log2 transformation for downstream pathway enrichment analysis. Hallmark pathways were downloaded as gene sets from MSigDB (36); MSigDB defines these as follows: hallmark gene sets summarize and represent specific well-defined biological states or processes and display coherent expression and were generated by a computational methodology based on identifying overlaps between gene sets in other MSigDB collections and retaining genes that display coordinate expression (37). Gene set enrichment analysis (GSEA) (103) was performed using the fgsea v1.18.0 package (104) in R to determine the normalized enrichment scores (NES) for each pathway along with the significance of the enrichment.

The average expression profile was also determined as a z score for the 31 genes identified above, and a heatmap was generated using the ComplexHeatmap v2.8.0 package (105).

For analysis of expression in Calu-3 cells infected with SARS-CoV-2 over time, the $\log_2$FC information at genome-wide scale was downloaded from GEO [GSE157490 (42)], and the mRNA data for Calu-3 cells infected with IAV over time were also downloaded from GEO [GSE76599 (43)]. Quantile normalization and $\log_2$ transformation were performed on the IAV mRNA data to obtain the $\log_2$FC for each gene by comparing the infection versus mock sample expression profiles. The "fgsea" function was then used to estimate the NES for IFN signaling pathways (IFN-α and IFN-γ responses) at each available time point for the SARS-CoV-2 and IAV infection, respectively.

For comparison of gene expression in the blood transcriptome between patients with SARS-CoV-2 infection and influenza and sepsis, RNA-seq data were downloaded from GEO [GSE163151 (40)]. Quality control steps were performed, including normalizing quantiles using the normalize.quantile function from preprocessCore, followed by $\log_2$ transformation. Comparisons were made for COVID-19 patient expression profiles versus healthy controls, sepsis versus healthy controls, and influenza versus healthy controls to determine the $\log_2$FC for all genes. The set of 50 aforementioned hallmark pathways and the $\log_2$FC information of each gene were used in the fgsea function to obtain the NES for each pathway. The average expression profile was also determined as a z score for the 31 consensus genes identified above, and a heatmap was generated.

Generation of Brie lentiviral library

The Mouse Brie CRISPR KO library was a gift from D. Root and J. Doench (Addgene, #73632 and #73633). The plasmid library was amplified and validated in the Center for Advanced Genome Engineering at St. Jude as described in the Broad GPP protocol, the only exception being the use of Endura DUOs electrocompetent cells. The St. Jude Hartwell Center Genome Sequencing Facility provided all next-generation sequencing. Single-end 100-cycle sequencing was performed on NovaSeq 6000 (Illumina). Validation to check guide RNA (gRNA) presence and representation was performed using calc_auc_v1.1.py (https://github.com/mhegde/) and count_spacers.py (106). Viral particles were produced by the St. Jude Vector Development and Production laboratory. CRISPR KO screens were analyzed using Mageck-Vispr/0.5.7 (107).

CRISPR-CAS9 library screen

CAS9-expressing iBMDMs generated from *Cas9-GFP* knock-in mice (108) were infected with the lentiviral particles at an MOI of 0.3. Two replicates of an adequate number of cells were used as control to obtain a representation (screen depth) of >500 cells for each single-guide RNA (sgRNA) of the library, and a similar number of cells from the same batch of virus preparation were infected with MHV at an MOI of 0.2 for 24 hours. The uninfected control cell population and the surviving cells from the MHV-infected samples were subjected to CRISPR screen enrichment analysis. Total genomic DNA was isolated using NucleoSpin Blood kits (Takara Bio Inc., USA, 740954 and 740950), and the concentrations of the isolated genomic DNA samples were measured using NanoDrop (Thermo Fisher Scientific, USA).

Using the MAGeCK pipeline (109), we robustly estimated the $\log_2$FC with significance of the essential genes from our CRISPR screen. The genes with positive fold change were imperative for cell death. The top gene hits along with their significance from the CRISPR screen were highlighted using a volcano plot.

Single-cell analysis

Single-cell data for comparisons of patients with COVID-19 versus healthy patients were obtained from FigShare (https://doi.org/10.6084/m9.figshare.14938755) (110). The dataset consisted of 268,745 cells: 114,201 cells from adults and 154,544 cells from children. Only data from adults were included in the final analysis. Additional metadata information was also obtained, including information about cell types and the two-dimensional coordinates of the Unified Manifold Approximation and Projection (UMAP) plot. "MC_Basophil," "Neutrophil," "mDC," "CD11c_mDC," "pDC," "moMa," "nrMa," "rMa," "NK," "IL17A_CD4," "IL17A_CD8," "CD8_Tm," "Treg," "B_cell," and "Plasma_cell" as defined in (110) were selected for further analyses, reducing the total number of cells to 19,361. Relabeling was performed: "MC_Basophil" → "Basophils," ["mDC," "CD11c_mDC," "pDC"] → "Dendritic cells," ["moMa," "nrMa," "rMa"] → "Macrophages," "NK" → "NK cells," "IL17A_CD4" → "CD4 T cells," ["IL17A_CD8," "CD8_Tm"] → "CD8 T cells," "B_cell" → "B cells," and "Plasma_cell" → "Plasma cells," respectively. The revised dataset contained 16,013 cells from patients with COVID-19 and 3348 healthy cells from adults. A nonparametric Mann-Whitney-Wilcoxon test (111) was used to compare average *ZBP1* expression across COVID-19 versus healthy cells.

Single-cell data for comparisons of patients with stable versus progressive COVID-19 were obtained from GEO [GSE155224 (69)]. The dataset consisted of 42,293 cells loaded using the Seurat v4.0.2 package (112). The SignacX v2.2.4 package (113) with default settings was used to annotate the cells as "B.memory," "B.naive," "DC," "Mon.Classical," "Neutrophils," "NK," "Plasma.cells," "T.CD4.memory," "T.CD4.naive," "T.CD8.cm," "T.CD8.em," "T.CD8.naive," "T.regs," and "Unclassified." Cell types having <500 cells were removed, including "Plasma.cells," "T.regs," and "T.CD8.cm" cells; those labeled as "Unclassified" were also removed. In total, 25,173 cells corresponding to six patients with stable COVID-19 and 13,248 cells corresponding to four patients with progressive COVID-19 were included. Relabeling was performed: "B.memory" → "B Memory," "B.naive" → "B Naive," "DC" → "Dendritic cells," "NK" → "NK cells," "T.CD4.memory" → "T CD4$^+$ Memory," "T.CD4.naive" → "T CD4$^+$ Naive," "T.CD8.cm" → "T CD8$^+$ CM," "T.CD8.em" → "T CD8$^+$ EM," and "T.CD8.naive" → "T CD8$^+$ Naive" cells, respectively. We then determined the average ZBP1 expression across patients with stable versus progressive COVID-19 bifurcated by the various cell states of interest.

Statistical analysis

GraphPad Prism 8.0 software was used for data analysis. Data are presented as means ± SEM. Statistical significance was determined by t tests (two-tailed) or Mann-Whitney-Wilcoxon test (nonparametric) for two groups or one-way or two-way analysis of variance (ANOVA) with multiple comparisons test for more groups. Survival analysis was performed using the log-rank (Mantel-Cox) test. $P < 0.05$ was considered statistically significant where $*P < 0.05$, $**P < 0.01$, $***P < 0.001$, and $****P < 0.0001$.

SUPPLEMENTARY MATERIALS
www.science.org/doi/10.1126/sciimmunol.abo6294

Figs. S1 to S8
Tables S1 and S2
MDAR Reproducibility Checklist

View/request a protocol for this paper from *Bio-protocol*.

REFERENCES AND NOTES

1. E. Dong, H. Du, L. Gardner, An interactive web-based dashboard to track COVID-19 in real time. *Lancet Infect. Dis.* **20**, 533–534 (2020).
2. J. J. V. Bavel, K. Baicker, P. S. Boggio, V. Capraro, A. Cichocka, M. Cikara, M. J. Crockett, A. J. Crum, K. M. Douglas, J. N. Druckman, J. Drury, O. Dube, N. Ellemers, E. J. Finkel, J. H. Fowler, M. Gelfand, S. Han, S. A. Haslam, J. Jetten, S. Kitayama, D. Mobbs, L. E. Napper, D. J. Packer, G. Pennycook, E. Peters, R. E. Petty, D. G. Rand, S. D. Reicher, S. Schnall, A. Shariff, L. J. Skitka, S. S. Smith, C. R. Sunstein, N. Tabri, J. A. Tucker, S. V. Linden, P. van Lange, K. A. Weeden, M. J. A. Wohl, J. Zaki, S. R. Zion, R. Willer, Using social and behavioural science to support COVID-19 pandemic response. *Nat. Hum. Behav.* **4**, 460–471 (2020).
3. C. Huang, Y. Wang, X. Li, L. Ren, J. Zhao, Y. Hu, L. Zhang, G. Fan, J. Xu, X. Gu, Z. Cheng, T. Yu, J. Xia, Y. Wei, W. Wu, X. Xie, W. Yin, H. Li, M. Liu, Y. Xiao, H. Gao, L. Guo, J. Xie, G. Wang, R. Jiang, Z. Gao, Q. Jin, J. Wang, B. Cao, Clinical features of patients infected with 2019 novel coronavirus in Wuhan, China. *Lancet* **395**, 497–506 (2020).
4. R. Karki, T. D. Kanneganti, The 'cytokine storm': Molecular mechanisms and therapeutic prospects. *Trends Immunol.* **42**, 681–705 (2021).
5. G. R. Stark, J. E. Darnell Jr., The JAK-STAT pathway at twenty. *Immunity* **36**, 503–514 (2012).
6. A. Wack, E. Terczyńska-Dyla, R. Hartmann, Guarding the frontiers: The biology of type III interferons. *Nat. Immunol.* **16**, 802–809 (2015).
7. J. M. Burke, L. A. St Clair, R. Perera, R. Parker, SARS-CoV-2 infection triggers widespread host mRNA decay leading to an mRNA export block. *RNA* **27**, 1318–1329 (2021).
8. G. Liu, J. H. Lee, Z. M. Parker, D. Acharya, J. J. Chiang, M. van Gent, W. Riedl, M. E. Davis-Gardner, E. Wies, C. Chiang, M. U. Gack, ISG15-dependent activation of the sensor MDA5 is antagonized by the SARS-CoV-2 papain-like protease to evade host innate immunity. *Nat. Microbiol.* **6**, 467–478 (2021).
9. J. Y. Li, C. H. Liao, Q. Wang, Y. J. Tan, R. Luo, Y. Qiu, X. Y. Ge, The ORF6, ORF8 and nucleocapsid proteins of SARS-CoV-2 inhibit type I interferon signaling pathway. *Virus Res.* **286**, 198074 (2020).
10. K. Chen, F. Xiao, D. Hu, W. Ge, M. Tian, W. Wang, P. Pan, K. Wu, J. Wu, SARS-CoV-2 nucleocapsid protein interacts with RIG-I and represses RIG-mediated IFN-β production. *Viruses* **13**, 47 (2020).
11. J. Wu, Y. Shi, X. Pan, S. Wu, R. Hou, Y. Zhang, T. Zhong, H. Tang, W. Du, L. Wang, J. Wo, J. Mu, Y. Qiu, K. Yang, L. K. Zhang, B. C. Ye, N. Qi, SARS-CoV-2 ORF9b inhibits RIG-I-MAVS antiviral signaling by interrupting K63-linked ubiquitination of NEMO. *Cell Rep.* **34**, 108761 (2021).
12. L. Han, M. W. Zhuang, J. Deng, Y. Zheng, J. Zhang, M. L. Nan, X. J. Zhang, C. Gao, P. H. Wang, SARS-CoV-2 ORF9b antagonizes type I and III interferons by targeting multiple components of the RIG-I/MDA-5-MAVS, TLR3-TRIF, and cGAS-STING signaling pathways. *J. Med. Virol.* **93**, 5376–5389 (2021).
13. L. Sui, Y. Zhao, W. Wang, P. Wu, Z. Wang, Y. Yu, Z. Hou, G. Tan, Q. Liu, SARS-CoV-2 membrane protein inhibits type I interferon production through ubiquitin-mediated degradation of TBK1. *Front. Immunol.* **12**, 662989 (2021).
14. M. Thoms, R. Buschauer, M. Ameismeier, L. Koepke, T. Denk, M. Hirschenberger, H. Kratzat, M. Hayn, T. Mackens-Kiani, J. Cheng, J. H. Straub, C. M. Stürzel, T. Fröhlich, O. Berninghausen, T. Becker, F. Kirchhoff, K. M. J. Sparrer, R. Beckmann, Structural basis for translational shutdown and immune evasion by the Nsp1 protein of SARS-CoV-2. *Science* **369**, 1249–1255 (2020).
15. J. C. Hsu, M. Laurent-Rolle, J. B. Pawlak, C. B. Wilen, P. Cresswell, Translational shutdown and evasion of the innate immune response by SARS-CoV-2 NSP14 protein. *Proc. Natl. Acad. Sci. U.S.A.* **118**, e2101161118 (2021).
16. H. Xia, Z. Cao, X. Xie, X. Zhang, J. Y. Chen, H. Wang, V. D. Menachery, R. Rajsbaum, P.-Y. Shi, Evasion of type I interferon by SARS-CoV-2. *Cell Rep.* **33**, 108234 (2020).
17. S. Wang, T. Dai, Z. Qin, T. Pan, F. Chu, L. Lou, L. Zhang, B. Yang, H. Huang, H. Lu, F. Zhou, Targeting liquid-liquid phase separation of SARS-CoV-2 nucleocapsid protein promotes innate antiviral immunity by elevating MAVS activity. *Nat. Cell Biol.* **23**, 718–732 (2021).
18. D. Blanco-Melo, B. E. Nilsson-Payant, W.-C. Liu, S. Uhl, D. Hoagland, R. Møller, T. X. Jordan, K. Oishi, M. Panis, D. Sachs, T. T. Wang, R. E. Schwartz, J. K. Lim, R. A. Albrecht, B. R. tenOever, Imbalanced host response to SARS-CoV-2 drives development of COVID-19. *Cell* **181**, 1036–1045.e9 (2020).
19. M. Li, M. Ferretti, B. Ying, H. Descamps, E. Lee, M. Dittmar, J. S. Lee, K. Whig, B. Kamalia, L. Dohnalová, G. Uhr, H. Zarkoob, Y.-C. Chen, H. Ramage, M. Ferrer, K. Lynch, D. C. Schultz, C. A. Thaiss, M. S. Diamond, S. Cherry, Pharmacological activation of STING blocks SARS-CoV-2 infection. *Sci. Immunol.* **6**, eabi9007 (2021).
20. F. Humphries, L. Shmuel-Galia, Z. Jiang, R. Wilson, P. Landis, S. L. Ng, K. M. Parsi, R. Maehr, J. Cruz, A. Morales-Ramos, J. M. Ramanjulu, J. Bertin, G. S. Pesiridis, K. A. Fitzgerald, A diamidobenzimidazole STING agonist protects against SARS-CoV-2 infection. *Sci. Immunol.* **6**, eabi9002 (2021).
21. W. Liu, H. M. Reyes, J. F. Yang, Y. Li, K. M. Stewart, M. C. Basil, S. M. Lin, J. Katzen, E. E. Morrisey, S. R. Weiss, J. You, Activation of STING signaling pathway effectively blocks human coronavirus infection. *J. Virol.* **95**, e00490-21 (2021).
22. T. Mao, B. Israelow, M. L. Gomez-Calvo, O. Fedorova, M. I. Breban, B. L. Menasche, H. Dong, M. Linehan; Yale SARS-CoV-2 Genome Surveillance Initiative, C. B. Wilen, M. L. Landry, N. D. Grubaugh, A. M. Pyle, A. Iwasaki, A stem-loop RNA RIG-I agonist protects against acute and chronic SARS-CoV-2 infection in mice. *J. Exp. Med.* **219**, e20211818 (2022).
23. P. Bessière, M. Wasniewski, E. Picard-Meyer, A. Servat, T. Figueroa, C. Foret-Lucas, A. Coggon, S. Lesellier, F. Boué, N. Cebron, B. Gausserès, C. Trumel, G. Foucras, F. J. Salguero, E. Monchatre-Leroy, R. Volmer, Intranasal type I interferon treatment is beneficial only when administered before clinical signs onset in the SARS-CoV-2 hamster model. *PLoS Pathog.* **17**, e1009427 (2021).
24. A. C. Kalil, A. K. Mehta, T. F. Patterson, N. Erdmann, C. A. Gomez, M. K. Jain, C. R. Wolfe, G. M. Ruiz-Palacios, S. Kline, J. R. Pineda, A. F. Luetkemeyer, M. S. Harkins, P. E. H. Jackson, N. M. Iovine, V. F. Tapson, M. D. Oh, J. A. Whitaker, R. A. Mularski, C. I. Paules, D. Ince, J. Takasaki, D. A. Sweeney, U. Sandkovsky, D. L. Wyles, E. Hohmann, K. A. Grimes, R. Grossberg, M. Laguio-Vila, A. A. Lambert, D. L. de Castilla, E. Kim, L. Larson, C. R. Wan, J. J. Traenkner, P. O. Ponce, J. E. Patterson, P. A. Goepfert, T. A. Sofarelli, S. Mocherla, E. R. Ko, A. P. de Leon, S. B. Doernberg, R. L. Atmar, R. C. Maves, F. Dangond, J. Ferreira, M. Green, M. Makowski, T. Bonnett, T. Beresnev, V. Ghazaryan, W. Dempsey, S. U. Nayak, L. Dodd, K. M. Tomashek, J. H. Beigel; ACTT-3 study group members, Efficacy of interferon beta-1a plus remdesivir compared with remdesivir alone in hospitalised adults with COVID-19: A double-blind, randomised, placebo-controlled, phase 3 trial. *Lancet Respir. Med.* **9**, 1365–1376 (2021).
25. N. Wang, Y. Zhan, L. Zhu, Z. Hou, F. Liu, P. Song, F. Qiu, X. Wang, X. Zou, D. Wan, X. Qian, S. Wang, Y. Guo, H. Yu, M. Cui, G. Tong, Y. Xu, Z. Zheng, Y. Lu, P. Hong, Retrospective multicenter cohort study shows early interferon therapy is associated with favorable clinical responses in COVID-19 patients. *Cell Host Microbe* **28**, 455–464.e2 (2020).
26. C. Lucas, P. Wong, J. Klein, T. B. R. Castro, J. Silva, M. Sundaram, M. K. Ellingson, T. Mao, J. E. Oh, B. Israelow, T. Takahashi, M. Tokuyama, P. Lu, A. Venkataraman, A. Park, S. Mohanty, H. Wang, A. L. Wyllie, C. B. F. Vogels, R. Earnest, S. Lapidus, I. M. Ott, A. J. Moore, M. C. Muenker, J. B. Fournier, M. Campbell, C. D. Odio, A. Casanovas-Massana; Yale IMPACT Team, R. Herbst, A. C. Shaw, R. Medzhitov, W. L. Schulz, N. D. Grubaugh, C. Dela Cruz, S. Farhadian, A. I. Ko, S. B. Omer, A. Iwasaki, Longitudinal analyses reveal immunological misfiring in severe COVID-19. *Nature* **584**, 463–469 (2020).
27. A. Zhou, X. Dong, M. Liu, B. Tang, Comprehensive transcriptomic analysis identifies novel antiviral factors against influenza A virus infection. *Front. Immunol.* **12**, 632798 (2021).
28. S. Balachandran, C. N. Kim, W. C. Yeh, T. W. Mak, K. Bhalla, G. N. Barber, Activation of the dsRNA-dependent protein kinase, PKR, induces apoptosis through FADD-mediated death signaling. *EMBO J.* **17**, 6888–6902 (1998).
29. R. Karki, B. Sundaram, B. R. Sharma, S. Lee, R. K. S. Malireddi, L. N. Nguyen, S. Christgen, M. Zheng, Y. Wang, P. Samir, G. Neale, P. Vogel, T. D. Kanneganti, ADAR1 restricts ZBP1-mediated immune response and PANoptosis to promote tumorigenesis. *Cell Rep.* **37**, 109858 (2021).
30. D. C. Fajgenbaum, C. H. June, Cytokine storm. *N. Engl. J. Med.* **383**, 2255–2273 (2020).
31. T. Kuriakose, S. M. Man, R. K. Malireddi, R. Karki, S. Kesavardhana, D. E. Place, G. Neale, P. Vogel, T. D. Kanneganti, ZBP1/DAI is an innate sensor of influenza virus triggering the NLRP3 inflammasome and programmed cell death pathways. *Sci. Immunol.* **1**, aag2045 (2016).
32. S. Kesavardhana, R. K. S. Malireddi, A. R. Burton, S. N. Porter, P. Vogel, S. M. Pruett-Miller, T.-D. Kanneganti, The Zα2 domain of ZBP1 is a molecular switch regulating influenza-induced PANoptosis and perinatal lethality during development. *J. Biol. Chem.* **295**, 8325–8330 (2020).
33. M. Devos, G. Tanghe, B. Gilbert, E. Dierick, M. Verheirstraeten, J. Nemegeer, R. De Reuver, S. Lefebvre, J. De Munck, J. Rehwinkel, P. Vandenabeele, W. Declercq, J. Maelfait, Sensing of endogenous nucleic acids by ZBP1 induces keratinocyte necroptosis and skin inflammation. *J. Exp. Med.* **217**, e20191913 (2020).
34. H. Jiao, L. Wachsmuth, S. Kumari, R. Schwarzer, J. Lin, R. O. Eren, A. Fisher, R. Lane, G. R. Young, G. Kassiotis, W. J. Kaiser, M. Pasparakis, Z-nucleic-acid sensing triggers ZBP1-dependent necroptosis and inflammation. *Nature* **580**, 391–395 (2020).
35. I. E. Galani, N. Rovina, V. Lampropoulou, V. Triantafyllia, M. Manioudaki, E. Pavlos, E. Koukaki, P. C. Fragkou, V. Panou, V. Rapti, O. Koltsida, A. Mentis, N. Koulouris, S. Tsiodras, A. Koutsoukou, E. Andreakos, Untuned antiviral immunity in COVID-19 revealed by temporal type I/III interferon patterns and flu comparison. *Nat. Immunol.* **22**, 32–40 (2021).
36. A. Subramanian, P. Tamayo, V. K. Mootha, S. Mukherjee, B. L. Ebert, M. A. Gillette, A. Paulovich, S. L. Pomeroy, T. R. Golub, E. S. Lander, J. P. Mesirov, Gene set enrichment

analysis: A knowledge-based approach for interpreting genome-wide expression profiles. *Proc. Natl. Acad. Sci. U.S.A.* **102**, 15545–15550 (2005).

37. A. Liberzon, C. Birger, H. Thorvaldsdóttir, M. Ghandi, J. P. Mesirov, P. Tamayo, The Molecular Signatures Database (MSigDB) hallmark gene set collection. *Cell Syst.* **1**, 417–425 (2015).

38. J. Xing, A. Zhang, Y. Du, M. Fang, L. J. Minze, Y. J. Liu, X. C. Li, Z. Zhang, Identification of poly(ADP-ribose) polymerase 9 (PARP9) as a noncanonical sensor for RNA virus in dendritic cells. *Nat. Commun.* **12**, 2681 (2021).

39. M. Miyashita, H. Oshiumi, M. Matsumoto, T. Seya, DDX60, a DEXD/H box helicase, is a novel antiviral factor promoting RIG-I-like receptor-mediated signaling. *Mol. Cell. Biol.* **31**, 3802–3819 (2011).

40. D. L. Ng, A. C. Granados, Y. A. Santos, V. Servellita, G. M. Goldgof, C. Meydan, A. Sotomayor-Gonzalez, A. G. Levine, J. Balcerek, L. M. Han, N. Akagi, K. Truong, N. M. Neumann, D. N. Nguyen, S. P. Bapat, J. Cheng, C. S. Martin, S. Federman, J. Foox, A. Gopez, T. Li, R. Chan, C. S. Chu, C. A. Wabl, A. S. Gliwa, K. Reyes, C. Y. Pan, H. Guevara, D. Wadford, S. Miller, C. E. Mason, C. Y. Chiu, A diagnostic host response biosignature for COVID-19 from RNA profiling of nasal swabs and blood. *Sci. Adv.* **7**, eabe5984 (2021).

41. F. McNab, K. Mayer-Barber, A. Sher, A. Wack, A. O'Garra, Type I interferons in infectious disease. *Nat. Rev. Immunol.* **15**, 87–103 (2015).

42. D. Kim, S. Kim, J. Park, H. R. Chang, J. Chang, J. Ahn, H. Park, J. Park, N. Son, G. Kang, J. Kim, K. Kim, M. S. Park, Y. K. Kim, D. Baek, A high-resolution temporal atlas of the SARS-CoV-2 translatome and transcriptome. *Nat. Commun.* **12**, 5120 (2021).

43. V. D. Menachery, A. Schäfer, K. E. Burnum-Johnson, H. D. Mitchell, A. J. Eisfeld, K. B. Walters, C. D. Nicora, S. O. Purvine, C. P. Casey, M. E. Monroe, K. K. Weitz, K. G. Stratton, B. M. Webb-Robertson, L. E. Gralinski, T. O. Metz, R. D. Smith, K. M. Waters, A. C. Sims, Y. Kawaoka, R. S. Baric, MERS-CoV and H5N1 influenza virus antagonize antigen presentation by altering the epigenetic landscape. *Proc. Natl. Acad. Sci. U.S.A.* **115**, E1012–E1021 (2018).

44. R. Channappanavar, A. R. Fehr, J. Zheng, C. Wohlford-Lenane, J. E. Abrahante, M. Mack, R. Sompallae, P. B. McCray Jr., D. K. Meyerholz, S. Perlman, IFN-I response timing relative to virus replication determines MERS coronavirus infection outcomes. *J. Clin. Invest.* **129**, 3625–3639 (2019).

45. R. Karki, B. R. Sharma, S. Tuladhar, E. P. Williams, L. Zalduondo, P. Samir, M. Zheng, B. Sundaram, B. Banoth, R. K. S. Malireddi, P. Schreiner, G. Neale, P. Vogel, R. Webby, C. B. Jonsson, T. D. Kanneganti, Synergism of TNF-α and IFN-γ triggers inflammatory cell death, tissue damage, and mortality in SARS-CoV-2 infection and cytokine shock syndromes. *Cell* **184**, 149–168.e17 (2021).

46. W. T. He, H. Wan, L. Hu, P. Chen, X. Wang, Z. Huang, Z. H. Yang, C. Q. Zhong, J. Han, Gasdermin D is an executor of pyroptosis and required for interleukin-1β secretion. *Cell Res.* **25**, 1285–1298 (2015).

47. J. Shi, Y. Zhao, K. Wang, X. Shi, Y. Wang, H. Huang, Y. Zhuang, T. Cai, F. Wang, F. Shao, Cleavage of GSDMD by inflammatory caspases determines pyroptotic cell death. *Nature* **526**, 660–665 (2015).

48. E. Obeng, Apoptosis (programmed cell death) and its signals—A review. *Braz. J. Biol.* **81**, 1133–1143 (2021).

49. S. A. Lakhani, A. Masud, K. Kuida, G. A. Porter Jr., C. J. Booth, W. Z. Mehal, I. Inayat, R. A. Flavell, Caspases 3 and 7: Key mediators of mitochondrial events of apoptosis. *Science* **311**, 847–851 (2006).

50. Y. K. Dhuriya, D. Sharma, Necroptosis: A regulated inflammatory mode of cell death. *J. Neuroinflammation* **15**, 199 (2018).

51. J. M. Murphy, P. E. Czabotar, J. M. Hildebrand, I. S. Lucet, J. G. Zhang, S. Alvarez-Diaz, R. Lewis, N. Lalaoui, D. Metcalf, A. I. Webb, S. N. Young, L. N. Varghese, G. M. Tannahill, E. C. Hatchell, I. J. Majewski, T. Okamoto, R. C. Dobson, D. J. Hilton, J. J. Babon, N. A. Nicola, A. Strasser, J. Silke, W. S. Alexander, The pseudokinase MLKL mediates necroptosis via a molecular switch mechanism. *Immunity* **39**, 443–453 (2013).

52. R. K. S. Malireddi, R. Karki, B. Sundaram, B. Kancharana, S. Lee, P. Samir, T. D. Kanneganti, Inflammatory cell death, PANoptosis, mediated by cytokines in diverse cancer lineages inhibits tumor growth. *Immunohorizons* **5**, 568–580 (2021).

53. B. Banoth, S. Tuladhar, R. Karki, B. R. Sharma, B. Briard, S. Kesavardhana, A. Burton, T.-D. Kanneganti, ZBP1 promotes fungi-induced inflammasome activation and pyroptosis, apoptosis, and necroptosis (PANoptosis). *J. Biol. Chem.* **295**, 18276–18283 (2020).

54. S. Christgen, M. Zheng, S. Kesavardhana, R. Karki, R. K. S. Malireddi, B. Banoth, D. E. Place, B. Briard, B. R. Sharma, S. Tuladhar, P. Samir, A. Burton, T.-D. Kanneganti, Identification of the PANoptosome: A molecular platform triggering pyroptosis, apoptosis, and necroptosis (PANoptosis). *Front. Cell. Infect. Microbiol.* **10**, 237 (2020).

55. R. Karki, B. R. Sharma, E. Lee, B. Banoth, R. K. S. Malireddi, P. Samir, S. Tuladhar, H. Mummareddy, A. R. Burton, P. Vogel, T.-D. Kanneganti, Interferon regulatory factor 1 regulates PANoptosis to prevent colorectal cancer. *JCI Insight* **5**, e136720 (2020).

56. M. Zheng, E. P. Williams, R. K. S. Malireddi, R. Karki, B. Banoth, A. Burton, R. Webby, R. Channappanavar, C. B. Jonsson, T.-D. Kanneganti, Impaired NLRP3 inflammasome activation/pyroptosis leads to robust inflammatory cell death via caspase-8/RIPK3 during coronavirus infection. *J. Biol. Chem.* **295**, 14040–14052 (2020).

57. P. Gurung, A. Burton, T.-D. Kanneganti, NLRP3 inflammasome plays a redundant role with caspase 8 to promote IL-1β–mediated osteomyelitis. *Proc. Natl. Acad. Sci. U.S.A.* **113**, 4452–4457 (2016).

58. J. R. Lukens, P. Gurung, P. Vogel, G. R. Johnson, R. A. Carter, D. J. McGoldrick, S. R. Bandi, C. R. Calabrese, L. Vande Walle, M. Lamkanfi, T. D. Kanneganti, Dietary modulation of the microbiome affects autoinflammatory disease. *Nature* **516**, 246–249 (2014).

59. R. K. Malireddi, S. Ippagunta, M. Lamkanfi, T. D. Kanneganti, Cutting edge: Proteolytic inactivation of poly(ADP-ribose) polymerase 1 by the Nlrp3 and Nlrc4 inflammasomes. *J. Immunol.* **185**, 3127–3130 (2010).

60. R. K. S. Malireddi, P. Gurung, S. Kesavardhana, P. Samir, A. Burton, H. Mummareddy, P. Vogel, S. Pelletier, S. Burgula, T.-D. Kanneganti, Innate immune priming in the absence of TAK1 drives RIPK1 kinase activity–independent pyroptosis, apoptosis, necroptosis, and inflammatory disease. *J. Exp. Med.* **217**, jem.20191644 (2020).

61. R. K. S. Malireddi, S. Kesavardhana, R. Karki, B. Kancharana, A. R. Burton, T. D. Kanneganti, RIPK1 distinctly regulates *Yersinia*-induced inflammatory cell death, PANoptosis. *Immunohorizons* **4**, 789–796 (2020).

62. R. K. S. Malireddi, P. Gurung, J. Mavuluri, T. K. Dasari, J. M. Klco, H. Chi, T. D. Kanneganti, TAK1 restricts spontaneous NLRP3 activation and cell death to control myeloid proliferation. *J. Exp. Med.* **215**, 1023–1034 (2018).

63. M. Zheng, R. Karki, P. Vogel, T.-D. Kanneganti, Caspase-6 is a key regulator of innate immunity, inflammasome activation, and host defense. *Cell* **181**, 674–687.e13 (2020).

64. M. Lamkanfi, T. D. Kanneganti, P. Van Damme, T. Vanden Berghe, I. Vanoverberghe, J. Vandekerckhove, P. Vandenabeele, K. Gevaert, G. Nuñez, Targeted peptidecentric proteomics reveals caspase-7 as a substrate of the caspase-1 inflammasomes. *Mol. Cell. Proteomics* **7**, 2350–2363 (2008).

65. P. Gurung, P. K. Anand, R. K. Malireddi, L. Vande Walle, N. Van Opdenbosch, C. P. Dillon, R. Weinlich, D. R. Green, M. Lamkanfi, T. D. Kanneganti, FADD and caspase-8 mediate priming and activation of the canonical and noncanonical Nlrp3 inflammasomes. *J. Immunol.* **192**, 1835–1846 (2014).

66. S. Lee, R. Karki, Y. Wang, L. N. Nguyen, R. C. Kalathur, T. D. Kanneganti, AIM2 forms a complex with pyrin and ZBP1 to drive PANoptosis and host defence. *Nature* **597**, 415–419 (2021).

67. M. Doerflinger, Y. Deng, P. Whitney, R. Salvamoser, S. Engel, A. J. Kueh, L. Tai, A. Bachem, E. Gressier, N. D. Geoghegan, S. Wilcox, K. L. Rogers, A. L. Garnham, M. A. Dengler, S. M. Bader, G. Ebert, J. S. Pearson, D. De Nardo, N. Wang, C. Yang, M. Pereira, C. E. Bryant, R. A. Strugnell, J. E. Vince, M. Pellegrini, A. Strasser, S. Bedoui, M. J. Herold, Flexible usage and interconnectivity of diverse cell death pathways protect against intracellular infection. *Immunity* **53**, 533–547.e7 (2020).

68. R. Wang, H. Li, J. Wu, Z.-Y. Cai, B. Li, H. Ni, X. Qiu, H. Chen, W. Liu, Z.-H. Yang, M. Liu, J. Hu, Y. Liang, P. Lan, J. Han, W. Mo, Gut stem cell necroptosis by genome instability triggers bowel inflammation. *Nature* **580**, 386–390 (2020).

69. A. A.-O. Unterman, T. A.-O. Sumida, N. A.-O. Nouri, X. Yan, A. Y. Zhao, V. A.-O. X. Gasque, J. A.-O. Schupp, H. Asashima, Y. Liu, C. Cosme Jr., W. Deng, M. Chen, M. A.-O. Raredon, K. A.-O. Hoehn, G. Wang, Z. A.-O. Wang, G. A.-O. Deluliis, N. A.-O. Ravindra, N. Li, C. Castaldi, P. Wong, J. Fournier, S. Bermejo, L. A.-O. Sharma, A. A.-O. Casanovas-Massana, C. A.-O. Vogels, A. A.-O. Wyllie, N. D. Grubaugh, A. Melillo, H. Meng, Y. A.-O. Stein, M. Minasyan, S. Mohanty, W. A.-O. Ruff, I. Cohen, K. Raddassi; The Yale IMPACT Research Team, L. E. Niklason, A. A.-O. Ko, R. A.-O. Montgomery, S. A.-O. Farhadian, A. A.-O. Iwasaki, A. C. Shaw, D. A.-O. van Dijk, H. A.-O. Zhao, S. A.-O. Kleinstein, V. A.-O. Hafler, N. A.-O. Kaminski, C. A.-O. Dela Cruz, Single-cell multi-omics reveals dyssynchrony of the innate and adaptive immune system in progressive COVID-19. *Nat. Commun.* **13**, 440 (2022).

70. M. Rebsamen, L. X. Heinz, E. Meylan, M. C. Michallet, K. Schroder, K. Hofmann, J. Vazquez, C. A. Benedict, J. Tschopp, DAI/ZBP1 recruits RIP1 and RIP3 through RIP homotypic interaction motifs to activate NF-κB. *EMBO Rep.* **10**, 916–922 (2009).

71. B. S. Graham, Rapid COVID-19 vaccine development. *Science* **368**, 945–946 (2020).

72. R. Forman, S. Shah, P. Jeurissen, M. Jit, E. Mossialos, COVID-19 vaccine challenges: What have we learned so far and what remains to be done? *Health Policy* **125**, 553–567 (2021).

73. RECOVERY Collaborative Group, P. Horby, W. S. Lim, J. R. Emberson, M. Mafham, J. L. Bell, L. Linsell, N. Staplin, C. Brightling, A. Ustianowski, E. Elmahi, B. Prudon, C. Green, T. Felton, D. Chadwick, K. Rege, C. Fegan, L. C. Chappell, S. N. Faust, T. Jaki, K. Jeffery, A. Montgomery, K. Rowan, E. Juszczak, J. K. Baillie, R. Haynes, M. J. Landray, Dexamethasone in hospitalized patients with Covid-19. *N. Engl. J. Med.* **384**, 693–704 (2021).

74. J. H. Beigel, K. M. Tomashek, L. E. Dodd, A. K. Mehta, B. S. Zingman, A. C. Kalil, E. Hohmann, H. Y. Chu, A. Luetkemeyer, S. Kline, D. L. de Castilla, R. W. Finberg, K. Dierberg, V. Tapson, L. Hsieh, T. F. Patterson, R. Paredes, D. A. Sweeney, W. R. Short, G. Touloumi, D. C. Lye, N. Ohmagari, M. D. Oh, G. M. Ruiz-Palacios, T. Benfield, G. Fätkenheuer, M. G. Kortepeter,

R. L. Atmar, C. B. Creech, J. Lundgren, A. G. Babiker, S. Pett, J. D. Neaton, T. H. Burgess, T. Bonnett, M. Green, M. Makowski, A. Osinusi, S. Nayak, H. C. Lane; ACTT-1 Study Group Members, Remdesivir for the treatment of Covid-19—Final report. *N. Engl. J. Med.* **383**, 1813–1826 (2020).

75. A. C. Kalil, T. F. Patterson, A. K. Mehta, K. M. Tomashek, C. R. Wolfe, V. Ghazaryan, V. C. Marconi, G. M. Ruiz-Palacios, L. Hsieh, S. Kline, V. Tapson, N. M. Iovine, M. K. Jain, D. A. Sweeney, H. M. El Sahly, A. R. Branche, J. R. Pineda, D. C. Lye, U. Sandkovsky, A. F. Luetkemeyer, S. H. Cohen, R. W. Finberg, P. E. H. Jackson, B. Taiwo, C. I. Paules, H. Arguinchona, P. Goepfert, N. Ahuja, M. Frank, M.-D. Oh, E. S. Kim, S. Y. Tan, R. A. Mularski, H. Nielsen, P. O. Ponce, B. S. Taylor, L. Larson, N. G. Rouphael, Y. Saklawi, V. D. Cantos, E. R. Ko, J. J. Engemann, A. N. Amin, M. Watanabe, J. Billings, M.-C. Elie, R. T. Davey, T. H. Burgess, J. Ferreira, M. Green, M. Makowski, A. Cardoso, S. De Bono, T. Bonnett, M. Proschan, G. A. Deye, W. Dempsey, S. U. Nayak, L. E. Dodd, J. H. Beigel; ACTT-2 Study Group Members, Baricitinib plus remdesivir for hospitalized adults with Covid-19. *N. Engl. J. Med.* **384**, 795–807 (2021).

76. J. Hammond, H. Leister-Tebbe, A. Gardner, P. Abreu, W. Bao, W. Wisemandle, M. Baniecki, V. M. Hendrick, B. Damle, A. Simón-Campos, R. Pypstra, J. M. Rusnak; EPIC-HR Investigators, Oral nirmatrelvir for high-risk, nonhospitalized adults with Covid-19. *N. Engl. J. Med.* **386**, 1397–1408 (2022).

77. A. Jayk Bernal, M. M. Gomes da Silva, D. B. Musungaie, E. Kovalchuk, A. Gonzalez, V. Delos Reyes, A. Martín-Quirós, Y. Caraco, A. Williams-Diaz, M. L. Brown, J. Du, A. Pedley, C. Assaid, J. Strizki, J. A. Grobler, H. H. Shamsuddin, R. Tipping, H. Wan, A. Paschke, J. R. Butterton, M. G. Johnson, C. De Anda; MOVe-OUT Study Group, Molnupiravir for oral treatment of Covid-19 in nonhospitalized patients. *N. Engl. J. Med.* **386**, 509–520 (2022).

78. D. A. Hoagland, R. Møller, S. A. Uhl, K. Oishi, J. Frere, I. Golynker, S. Horiuchi, M. Panis, D. Blanco-Melo, D. Sachs, K. Arkun, J. K. Lim, B. R. tenOever, Leveraging the antiviral type I interferon system as a first line of defense against SARS-CoV-2 pathogenicity. *Immunity* **54**, 557–570.e5 (2021).

79. Q. Zhu, Y. Zhang, L. Wang, X. Yao, D. Wu, J. Cheng, X. Pan, H. Liu, Z. Yan, L. Gao, Inhibition of coronavirus infection by a synthetic STING agonist in primary human airway system. *Antiviral Res.* **187**, 105015 (2021).

80. Q. Zhou, V. Chen, C. P. Shannon, X. S. Wei, X. Xiang, X. Wang, Z. H. Wang, S. J. Tebbutt, T. R. Kollmann, E. N. Fish, Interferon-α2b treatment for COVID-19. *Front. Immunol.* **11**, 1061 (2020).

81. I. F. Hung, K. C. Lung, E. Y. Tso, R. Liu, T. W. Chung, M. Y. Chu, Y. Y. Ng, J. Lo, J. Chan, A. R. Tam, H. P. Shum, V. Chan, A. K. Wu, K. M. Sin, W. S. Leung, W. L. Law, D. C. Lung, S. Sin, P. Yeung, C. C. Yip, R. R. Zhang, A. Y. Fung, E. Y. Yan, K. H. Leung, J. D. Ip, A. W. Chu, W. M. Chan, A. C. Ng, R. Lee, K. Fung, A. Yeung, T. C. Wu, J. W. Chan, W. W. Yan, W. M. Chan, J. F. Chan, A. K. Lie, O. T. Tsang, V. C. Cheng, T. L. Que, C. S. Lau, K. H. Chan, K. K. To, K. Y. Yuen, Triple combination of interferon beta-1b, lopinavir–ritonavir, and ribavirin in the treatment of patients admitted to hospital with COVID-19: An open-label, randomised, phase 2 trial. *Lancet* **395**, 1695–1704 (2020).

82. E. Davoudi-Monfared, H. Rahmani, H. Khalili, M. Hajiabdolbaghi, M. Salehi, L. Abbasian, H. Kazemzadeh, M. S. Yekaninejad, A randomized clinical trial of the efficacy and safety of interferon β-1a in treatment of severe COVID-19. *Antimicrob. Agents Chemother.* **64**, e01061-20 (2020).

83. H. Rahmani, E. Davoudi-Monfared, A. Nourian, H. Khalili, N. Hajizadeh, N. Z. Jalalabadi, M. R. Fazeli, M. Ghazaeian, M. S. Yekaninejad, Interferon β-1b in treatment of severe COVID-19: A randomized clinical trial. *Int. Immunopharmacol.* **88**, 106903 (2020).

84. WHO Solidarity Trial Consortium, H. Pan, R. Peto, A. M. Henao-Restrepo, M. P. Preziosi, V. Sathiyamoorthy, Q. A. Karim, M. M. Alejandria, C. H. García, M. P. Kieny, R. Malekzadeh, S. Murthy, K. S. Reddy, M. R. Periago, P. A. Hanna, F. Ader, A. M. Al-Bader, A. Alhasawi, E. Allum, A. Alotaibi, C. A. Alvarez-Moreno, S. Appadoo, A. Asiri, P. Aukrust, A. Barratt-Due, S. Bellani, M. Branca, H. B. C. Cappel-Porter, N. Cerrato, T. S. Chow, N. Como, J. Eustace, P. J. García, S. Godbole, E. Gotuzzo, L. Griskevicius, R. Hamra, M. Hassan, M. Hassany, D. Hutton, I. Irmansyah, L. Jancoriene, J. Kirwan, S. Kumar, P. Lennon, G. Lopardo, P. Lydon, N. Magrini, T. Maguire, S. Manevska, O. Manuel, S. McGinty, M. T. Medina, M. L. M. Rubio, M. C. Miranda-Montoya, J. Nel, E. P. Nunes, M. Perola, A. Portolés, M. R. Rasmin, A. Raza, H. Rees, P. P. S. Reges, C. A. Rogers, K. Salami, M. I. Salvadori, N. Sinani, J. A. C. Sterne, M. Stevanovikj, E. Tacconelli, K. A. O. Tikkinen, S. Trelle, H. Zaid, J. A. Røttingen, S. Swaminathan, Repurposed antiviral drugs for Covid-19 - interim WHO solidarity trial results. *N. Engl. J. Med.* **384**, 497–511 (2021).

85. F. Ader, N. Peiffer-Smadja, J. Poissy, M. Bouscambert-Duchamp, D. Belhadi, A. Diallo, C. Delmas, J. Saillard, A. Dechanet, N. Mercier, A. Dupont, T. Alfaiate, F. X. Lescure, F. Raffi, F. Goehringer, A. Kimmoun, S. Jaureguiberry, J. Reignier, S. Nseir, F. Danion, R. Clere-Jehl, K. Bouiller, J. C. Navellou, V. Tolsma, A. Cabié, C. Dubost, J. Courjon, S. Leroy, J. Mootien, R. Gaci, B. Mourvillier, E. Faure, V. Pourcher, S. Gallien, O. Launay, K. Lacombe, J. P. Lanoix, A. Makinson, G. Martin-Blondel, L. Bouadma, E. Botelho-Nevers, A. Gagneux-Brunon, O. Epaulard, L. Piroth, F. Wallet, J. C. Richard, J. Reuter, T. Staub, B. Lina, M. Noret, C. Andrejak, M. P. Lê, G. Peytavin, M. Hites, D. Costagliola, Y. Yazdanpanah, C. Burdet,
F. Mentré; DisCoVeRy study group, An open-label randomized controlled trial of the effect of lopinavir/ritonavir, lopinavir/ritonavir plus IFN-β-1a and hydroxychloroquine in hospitalized patients with COVID-19. *Clin. Microbiol. Infect.* **27**, 1826–1837 (2021).

86. C. M. Silva, C. W. S. Wanderley, F. P. Veras, A. V. Gonçalves, M. H. F. Lima, J. E. T. Kawahisa, G. F. Gomes, D. C. Nascimento, V. V. S. Monteiro, I. M. Paiva, C. J. L. R. Almeida, D. B. Caetité, J. D. C. Silva, M. I. F. Lopes, L. P. Bonjorno, M. C. Giannini, N. B. Amaral, M. N. Benatti, L. E. A. Damasceno, B. M. S. Silva, A. H. Schneider, I. M. S. Castro, J. C. S. Silva, A. P. Vasconcelos, T. T. Gonçalves, S. S. Batah, T. S. Rodrigues, V. F. Costa, M. C. Pontelli, R. B. Martins, T. V. Martins, D. L. A. Espósito, G. C. M. Cebinelli, B. A. L. da Fonseca, L. O. S. Leiria, L. D. Cunha, E. Arruda, H. I. Nakaia, A. T. Fabro, R. D. Oliveira, D. S. Zamboni, P. L. Junior, T. M. Cunha, J. C. F. A. Filho, F. D. Q. Cunha, Gasdermin-D activation by SARS-CoV-2 trigger NET and mediate COVID-19 immunopathology. *medRxiv* 10.1101/2022.2001.2024.22269768 (2022).

87. J. Major, S. Crotta, M. Llorian, T. M. McCabe, H. H. Gad, S. L. Priestnall, R. Hartmann, A. Wack, Type I and III interferons disrupt lung epithelial repair during recovery from viral infection. *Science* **369**, 712–717 (2020).

88. R. J. Thapa, J. P. Ingram, K. B. Ragan, S. Nogusa, D. F. Boyd, A. A. Benitez, H. Sridharan, R. Kosoff, M. Shubina, V. J. Landsteiner, M. Andrake, P. Vogel, L. J. Sigal, B. R. tenOever, P. G. Thomas, J. W. Upton, S. Balachandran, DAI senses influenza A virus genomic RNA and activates RIPK3-dependent cell death. *Cell Host Microbe* **20**, 674–681 (2016).

89. M. Momota, P. Lelliott, A. Kubo, T. Kusakabe, K. Kobiyama, E. Kuroda, Y. Imai, S. Akira, C. Coban, K. J. Ishii, ZBP1 governs the inflammasome-independent IL-1α and neutrophil inflammation that play a dual role in anti-influenza virus immunity. *Int. Immunol.* **32**, 203–212 (2020).

90. J. A.-O. Di Domizio, M. F. Gulen, F. Saidoune, V. A.-O. X. Thacker, A. Yatim, K. A.-O. Sharma, T. A.-O. Nass, E. A.-O. Guenova, M. Schaller, C. A.-O. Conrad, C. Goepfert, L. A.-O. X. De Leval, C. von Garnier, S. Berezowska, A. A.-O. Dubois, M. A.-O. Gilliet, A. A.-O. Ablasser, The cGAS–STING pathway drives type I IFN immunopathology in COVID-19. *Nature* **603**, 145–151 (2022).

91. K. J. Ishii, T. Kawagoe, S. Koyama, K. Matsui, H. Kumar, T. Kawai, S. Uematsu, O. Takeuchi, F. Takeshita, C. Coban, S. Akira, TANK-binding kinase-1 delineates innate and adaptive immune responses to DNA vaccines. *Nature* **451**, 725–729 (2008).

92. K. Newton, X. Sun, V. M. Dixit, Kinase RIP3 is dispensable for normal NF-kappa Bs, signaling by the B-cell and T-cell receptors, tumor necrosis factor receptor 1, and Toll-like receptors 2 and 4. *Mol. Cell. Biol.* **24**, 1464–1469 (2004).

93. A. Oberst, C. P. Dillon, R. Weinlich, L. L. McCormick, P. Fitzgerald, C. Pop, R. Hakem, G. S. Salvesen, D. R. Green, Catalytic activity of the caspase-8-FLIP(L) complex inhibits RIPK3-dependent necrosis. *Nature* **471**, 363–367 (2011).

94. M. E. Grunewald, A. R. Fehr, J. Athmer, S. Perlman, The coronavirus nucleocapsid protein is ADP-ribosylated. *Virology* **517**, 62–68 (2018).

95. J. H. Schickli, B. D. Zelus, D. E. Wentworth, S. G. Sawicki, K. V. Holmes, The murine coronavirus mouse hepatitis virus strain A59 from persistently infected murine cells exhibits an extended host range. *J. Virol.* **71**, 9499–9507 (1997).

96. R. E. Tweedell, R. K. S. Malireddi, T. D. Kanneganti, A comprehensive guide to studying inflammasome activation and cell death. *Nat. Protoc.* **15**, 3284–3333 (2020).

97. T. Ebisudani, S. Sugimoto, K. Haga, A. Mitsuishi, R. Takai-Todaka, M. Fujii, K. Toshimitsu, J. Hamamoto, K. Sugihara, T. Hishida, H. Asamura, H. Yasuda, K. Katayama, T. Sato, Direct derivation of human alveolospheres for SARS-CoV-2 infection modeling and drug screening. *Cell Rep.* **35**, 109218 (2021).

98. K. A. Overmyer, E. Shishkova, I. J. Miller, J. Balnis, M. N. Bernstein, T. M. Peters-Clarke, J. G. Meyer, Q. Quan, L. K. Muehlbauer, E. A. Trujillo, Y. He, A. Chopra, H. C. Chieng, A. Tiwari, M. A. Judson, B. Paulson, D. R. Brademan, Y. Zhu, L. R. Serrano, V. Linke, L. A. Drake, A. P. Adam, B. S. Schwartz, H. A. Singer, S. Swanson, D. F. Mosher, R. Stewart, J. J. Coon, A. Jaitovich, Large-scale multi-omic analysis of COVID-19 severity. *Cell Syst.* **12**, 23–40.e7 (2021).

99. Y. Lévy, A. Wiedemann, B. P. Hejblum, M. Durand, C. Lefebvre, M. Surénaud, C. Lacabaratz, M. Perreau, E. Foucat, M. Déchenaud, P. Tisserand, F. Blengio, B. Hivert, M. Gauthier, M. Cervantes-Gonzalez, D. Bachelet, C. Laouénan, L. Bouadma, J. F. Timsit, Y. Yazdanpanah, G. Pantaleo, H. Hocini, R. Thiébaut; French COVID cohort study group, CD177, a specific marker of neutrophil activation, is associated with coronavirus disease 2019 severity and death. *iScience* **24**, 102711 (2021).

100. M. I. Love, W. Huber, S. Anders, Moderated estimation of fold change and dispersion for RNA-seq data with DESeq2. *Genome Biol.* **15**, 550 (2014).

101. M. E. Ritchie, B. Phipson, D. Wu, Y. Hu, C. W. Law, W. Shi, G. K. Smyth, *limma* powers differential expression analyses for RNA-sequencing and microarray studies. *Nucleic Acids Res.* **43**, e47 (2015).

102. Y. Benjamini, Y. Hochberg, Controlling the false discovery rate: A practical and powerful approach to multiple testing. *J. R. Stat. Soc. B Methodol.* **57**, 289–300 (1995).

103. V. K. Mootha, J. Bunkenborg, J. V. Olsen, M. Hjerrild, J. R. Wisniewski, E. Stahl, M. S. Bolouri, H. N. Ray, S. Sihag, M. Kamal, N. Patterson, E. S. Lander, M. Mann, Integrated analysis

of protein composition, tissue diversity, and gene regulation in mouse mitochondria. *Cell* **115**, 629–640 (2003).

104. A. A. Sergushichev, An algorithm for fast preranked gene set enrichment analysis using cumulative statistic calculation. bioRxiv 060012 [**Preprint**]. 20 June 2016. https://doi.org/10.1101/060012.

105. Z. Gu, R. Eils, M. Schlesner, Complex heatmaps reveal patterns and correlations in multidimensional genomic data. *Bioinformatics* **32**, 2847–2849 (2016).

106. J. Joung, S. Konermann, J. S. Gootenberg, O. O. Abudayyeh, R. J. Platt, M. D. Brigham, N. E. Sanjana, F. Zhang, Genome-scale CRISPR-Cas9 knockout and transcriptional activation screening. *Nat. Protoc.* **12**, 828–863 (2017).

107. W. Li, J. Köster, H. Xu, C. H. Chen, T. Xiao, J. S. Liu, M. Brown, X. S. Liu, Quality control, modeling, and visualization of CRISPR screens with MAGeCK-VISPR. *Genome Biol.* **16**, 281 (2015).

108. R. J. Platt, S. Chen, Y. Zhou, M. J. Yim, L. Swiech, H. R. Kempton, J. E. Dahlman, O. Parnas, T. M. Eisenhaure, M. Jovanovic, D. B. Graham, S. Jhunjhunwala, M. Heidenreich, R. J. Xavier, R. Langer, D. G. Anderson, N. Hacohen, A. Regev, G. Feng, P. A. Sharp, F. Zhang, CRISPR-Cas9 knockin mice for genome editing and cancer modeling. *Cell* **159**, 440–455 (2014).

109. W. Li, H. Xu, T. Xiao, L. Cong, M. I. Love, F. Zhang, R. A. Irizarry, J. S. Liu, M. Brown, X. S. Liu, MAGeCK enables robust identification of essential genes from genome-scale CRISPR/Cas9 knockout screens. *Genome Biol.* **15**, 554 (2014).

110. J. Loske, J. Röhmel, S. Lukassen, S. Stricker, V. G. Magalhães, J. Liebig, R. L. Chua, L. Thürmann, M. Messingschlager, A. Seegebarth, B. Timmermann, S. Klages, M. Ralser, B. Sawitzki, L. E. Sander, V. M. Corman, C. Conrad, S. Laudi, M. Binder, S. Trump, R. Eils, M. A. Mall, I. Lehmann, Pre-activated antiviral innate immunity in the upper airways controls early SARS-CoV-2 infection in children. *Nat. Biotechnol.* **40**, 319–324 (2022).

111. T. M. Hettmansperger, J. W. McKean, *Robust Nonparametric Statistical Methods* (CRC Press, ed. 2, 2010).

112. Y. Hao, S. Hao, E. Andersen-Nissen, W. M. Mauck III, S. Zheng, A. Butler, M. J. Lee, A. J. Wilk, C. Darby, M. Zager, P. Hoffman, M. Stoeckius, E. Papalexi, E. P. Mimitou, J. Jain, A. Srivastava, T. Stuart, L. M. Fleming, B. Yeung, A. J. Rogers, J. M. McElrath, C. A. Blish, R. Gottardo, P. Smibert, R. Satija, Integrated analysis of multimodal single-cell data. *Cell* **184**, 3573–3587.e29 (2021).

113. S. Virginia, C. Mathew, H. Richa, N. Frank, R. de Emanuele, Cell type classification and discovery across diseases, technologies and tissues reveals conserved gene signatures and enables standardized single-cell readouts. *Res. Square* (2021).

Science Immunology

ZBP1-dependent inflammatory cell death, PANoptosis, and cytokine storm disrupt IFN therapeutic efficacy during coronavirus infection

Rajendra KarkiSangJoon LeeRaghvendra MallNagakannan PandianYaqiu WangBhesh Raj SharmaRK Subbarao MalireddiDong YangSanja TrifkovicJacob A. SteeleJon P. ConnellyGella VishwanathMitnala SasikalaDuvvur Nageshwar ReddyPeter VogelShondra M. Pruett-MillerRichard WebbyColleen Beth JonssonThirumala-Devi Kanneganti

ZBP1 fans the flames of cytokine storm

Type I interferons (IFNs) provide robust innate immune protection against #-coronaviruses including SARS-CoV-2 when available soon after infection. Paradoxically, therapeutic use of type I IFNs in patients with severe COVID-19 may promote increased pathology and clinical deterioration. Using a mouse model of respiratory #-coronavirus infection with mouse hepatitis virus (MHV), Karki *et al.* found that the detrimental effects of type I IFNs in later stages of infection were related to IFN-induced expression of ZBP1, an innate immune sensor also capable of inducing PANoptosis, an inflammatory form of cell death. Mice lacking ZBP1 were protected from IFN-induced lethality in the MHV infection model. These findings suggest that ZBP1 could be targeted therapeutically in severe COVID-19 to ward off deleterious effects of type I IFNs including cytokine storm.

View the article online
https://www.science.org/doi/10.1126/sciimmunol.abo6294
Permissions
https://www.science.org/help/reprints-and-permissions